Supplementary Information for

Bioinspired neuron-like electronics

Xiao Yang[1]†, Tao Zhou[1]†, Theodore J. Zwang[1]†, Guosong Hong[1], Yunlong Zhao[1], Robert D. Viveros[3], Tian-Ming Fu[1], Teng Gao[1] and Charles M. Lieber[1,2,3]*

[1]Department of Chemistry and Chemical Biology, Harvard University, Cambridge, Massachusetts, USA.

[2]Center for Brain Science, Harvard University, Cambridge, Massachusetts, USA.

[3]John A. Paulson School of Engineering and Applied Sciences, Harvard University, Cambridge, Massachusetts, USA.

*Correspondence to: cml@cmliris.harvard.edu.

†These authors contributed equally to this work.

Table of Contents:

1. Bending stiffness calculations.

We estimated and compared the bending stiffness, D, values of the NeuE and axons using a beam model[53]. The bending stiffness of NeuE can be estimated as $D = \frac{Ewh^3}{12}$. Taking into account the three-layer polymer/metal/polymer structure of the unit of the NeuE, $D = \frac{E_S}{12}(wh^3 - w_m h_m^3) + \frac{E_m}{12}w_m h_m^3$, where E_S and E_m are the Young's moduli of SU-8 and gold, 2 and 79 GPa, respectively[16], w is the total width of the neurite-like interconnect and w_m is the width of metal. NeuE designs 1 and 2 (Supplementary Table 1) both with $h = 940$ nm and $h_m = 100$ nm yield $D_{NeuE1} = 5.7 \times 10^{-16}$ N $\cdot$ m^2 and $D_{NeuE2} = 1.4 \times 10^{-16}$ N $\cdot$ m^2. These NeuE values fall within the range estimated for axons, where $E_{axon} = 12$ MPa [23] and $d_{axon} = 1\sim6$ μm [24] yield $D_{axon} = E_{axon}\frac{\pi d_{axon}^4}{64} = 5.9 \times 10^{-19}\sim7.6 \times 10^{-16}$ N $\cdot$ m^2.

In addition, D-values for reported state-of-the-art probes[17,19,20,22] with the lowest reported values are compared as a reference: (1) our previously reported mesh electronics design[17], $w = 20$ μm and $w_m = 10$ μm, $D_{Mesh} = 2.8 \times 10^{-15}$ N $\cdot$ m^2; (2) the nanoelectronic electrodes that Luan, L. et al reported[22], $w_{NET-50} = 50$ μm, $h_{NET-50} = 1$ μm, $D_{NET-50} = 8.3 \times 10^{-15}$ N $\cdot$ m^2; $w_{NET-10} = 10$ μm, $h_{NET-10} = 1.5$ μm, $D_{NET-10} = 5.6 \times 10^{-15}$ N $\cdot$ m^2; and (3) the fiber probes reported by Canales, A. et $al.$[20] and Park. S. et $al.$[21] can be estimated as $D_{fiber} = E_{fiber}\frac{\pi d_{fiber}^4}{64}$, and $E_{fiber} = 1.7$ GPa [54] and minimum $d_{fiber} = 70$ μm yield $D_{fiber} = 2.0 \times 10^{-9}$ N $\cdot$ m^2. The key parameter changes which lead to substantially reduced bending stiffness result from the unique structure of NeuE. Specifically, the reduction in longitudinal and transverse element widths from 20 μm of a cell soma to 4 μm for NeuE-1 and 1 μm for NeuE-2 designs of neurites, resulted in the 5 and 20-fold decreases.

2. 2D and 3D porosity calculations.

The 2D and 3D porosity of NeuE probes shown in Supplementary Table 1 were estimated using their structural parameters. 3D porosity also uses the diameter of NeuE as 200 μm, a typical value revealed by 3D imaging.

3. Success rate for surgery.

The success (failure) rate for surgery leading to stable tissue interface and electrophysiological recording was ca. 80% (20%). There are two principal factors that can result in failed surgeries. (1) The total injection volume, which is usually 5-50 μL over ca. 2 mm length of injection, is >50 μL during the implantation procedure. In these cases the animal is excluded from the study since excess solution can result in brain edema or other damage. (2) Animals where there was accidental damage of a more major blood vessel, which is indicated by significant bleeding during surgery, were also excluded from our study.

4. Image data analysis.

ZEN software (Carl Zeiss Microscopy GmbH, Jena, Germany) was used for stitching tile scan images. Imaris 9 software (Bitplane, Zurich, Switzerland) was used for neuron tracing, segmentation, color rendering and generating animation videos. A combination of Imaris, ImageJ (National Institutes of Health, Bethesda, MD) and MATLAB (MathWorks, Natick, MA) was used for quantitative analysis of fluorescence intensity as a function of the distance from the 3D NeuE boundary. Imaris was used to define the smallest 3D boundary that encompasses all the NeuE structure. This 3D boundary separates all voxels into 'interior' voxels and 'exterior' voxels. Imaris was also used to define the 3D volume of each brain region according to their specific shape. The

typical thickness of the 3D volume of each brain region is 500 ± 100 μm. ImageJ was used to export fluorescence intensities, distances from the 3D boundary and associated 3D coordinates in matrix format that was later imported into MATLAB. MATLAB was used to calculate fluorescence intensity as a function of the distance from the 3D boundary. (**1**) For the quantitative analysis in Fig. 2, the intensity values for all voxels with distances binned over an interval of 20 μm were averaged and normalized against the baseline value defined as the average fluorescence intensity of all background voxels 480-500 μm away from the 3D NeuE boundary. (**2**) The analysis procedure for Supplementary Fig. 5d was similar to (1). In this case, the baseline value was defined as the average fluorescence intensity of all background voxels 420-440 μm away from the 3D NeuE boundary. (**3**) The analysis procedure for Supplementary Fig. 7a,b was similar to (1). In this case, the baseline value was defined as the average fluorescence intensity of all background voxels 440-460 μm away from the 3D NeuE boundary, except that 420-440 μm was used for baseline of neuron intensity in the cortex; 380-400 μm was used as baseline of astrocyte intensity in the DG and 420-440 μm was used for baseline of astrocyte intensity in the CA1 at 2 weeks post-implantation due to too few voxels farther away to serve as reliable baseline. (**4**) The analysis procedure for Supplementary Fig. 7c,d was similar to (1). For neuron intensity (c), the baseline value was defined as the average fluorescence intensity of all background voxels 460-480 μm away from the 3D NeuE boundary, except that 420-440 μm was used as baseline in the DG at 6 weeks and in the CTX at 12 weeks post-implantation due to too few voxels farther away to serve as reliable baseline. For astrocyte intensity (d), the baseline value was defined as the average fluorescence intensity of all background voxels 440-460 μm away from the 3D NeuE boundary, except that 400-420 μm was used as baseline in the CTX at 6 weeks post-implantation due to too few voxels farther away to serve as reliable baseline. (**5**) The analysis procedure for Fig. 4c was

4

similar to (1). In this case, the normalized fluorescence intensity was defined as the ratio of the average fluorescence intensity of all voxels from NeuE elements or 20 μm control mesh elements to 20 μm away versus the baseline value as the average fluorescence intensity of all voxels 260-280 μm away. (**6**) The quantitative analysis of intact tissues without implantation, as shown in Supplementary Fig. 9, was done in a similar way using an arbitrary vertical line as a proxy for the probe, as indicated with the vertical white dashed lines, that pass through CTX, CA1 and DG. The baseline value was defined as the fluorescence intensity averaged over a range of 480-500 μm away. (**7**) The quantitative analysis of sham injection samples without NeuE implantation, as shown in Supplementary Fig. 10, was done in a similar way, where the fluorescence intensity within the needle insertion track (indicated with the white dashed box) versus the background was calculated by taking the average fluorescence intensity within the volume of needle insertion track and dividing it by the baseline fluorescence intensity 340-440 μm away from the injection site.

The 50-μm thick horizontal slices shown in Supplementary Fig. 8b were extracted at distinct brain regions from the optically reconstructed 3D images by Imaris software. The quantitative analysis of fluorescence intensity as a function of the distance from the NeuE boundary shown in Supplementary Fig. 8e,f was calculated using MATLAB in a similar manner as described previously[18] and the baseline value was defined as the fluorescence intensity averaged over a range of 480-500 μm away from NeuE probe.

5. Analysis of recorded electrophysiological data.

5.1. Analysis of single-unit activity. The recorded data were analyzed offline in a similar manner to our previous report[17,25,55]. In brief, raw recording data were filtered using the 'filtfilt' function in MATLAB in the 250–6,000 Hz frequency range to extract single-unit spikes. Single-unit spike

sorting was performed by amplitude thresholding of the filtered traces, automatically determining the threshold based on the median of the background noise with the improved noise estimation method[36]. The SNR for each recording channel was calculated by dividing the average peak-to-peak amplitude of all sorted spikes by noise derived from noise estimation of a typical 1-min recording trace. Sorted spikes were clustered to determine the number of single neurons and to assign spikes to each single neuron based on principal component analysis (PCA) using the WaveClus 2.0 program that employs unsupervised superparamagnetic clustering of single-unit spikes[36].

To assess the quality of cluster separation, the L-ratio for each cluster of spikes was calculated as follows[37],

$$L_{ratio} = \frac{L(C)}{N(C)} = \frac{\sum_{i \notin C} 1 - CDF_{\chi^2}(D_{i,C}^2)}{N(C)}$$

(1)

Where $N(C)$ denotes the number of spikes in the cluster, CDF_{χ^2} presents the cumulative distribution function of the χ^2 distribution, and $D_{i,C}^2$ is the Mahalanobis distance of a spike i from the center of the cluster C. An L-ratio of < 0.05 is considered good cluster separation/isolation[37,38]. As shown in the Supplementary Table 3, the L-ratios demonstrate that single units are well separated.

The autocorrelation of average spike waveforms shown in Supplementary Fig. 17 was computed based on the standard Pearson product-moment correlation coefficient as follows,

$$Corr(Y_1, Y_2) = \frac{\int_0^T (Y_1(t) - \overline{Y_1})(Y_2(t) - \overline{Y_2})dt}{\sqrt{\int_0^T (Y_1(t) - \overline{Y_1})^2(Y_2(t) - \overline{Y_2})^2 dt}}$$

(2)

Where $Y_1(t)$ and $Y_2(t)$ are two spike waveforms with a duration T at different days[34]. The correlation histograms show the percentage distributions of correlation coefficients (i.e., waveform similarity) defined in Equation (2) for all pairwise comparisons between the average spike waveforms within the same group. A value of 1 indicates identical spike shapes.

5.2. Resolving neuron locations by triangulation. First, pairwise cross-correlation analysis was performed between identified neurons from different channels. The cross-correlation analysis between neurons was achieved through MATLAB software. According to the spike timestamps of each of the identified neurons after spike sorting and clustering, the original high-pass filtered recording traces were turned into binary spike trains with a '1' indicating a firing event and a '0' indicating a non-firing event. Then the binary spike trains were subjected to standard Pearson product-moment correlation coefficient analysis between every pair, as follows:

$$Corr(Y_1, Y_2, \Delta t) = \frac{\int_0^T (Y_1(t) - \overline{Y_1})(Y_2(t - \Delta t) - \overline{Y_2})dt}{\sqrt{\int_0^T (Y_1(t) - \overline{Y_1})^2 (Y_2(t - \Delta t) - \overline{Y_2})^2 dt}}$$

(3)

Where $Y_1(t)$ and $Y_2(t)$ represent the firing events of two PCA-clustered neurons, t represents the duration of recording and Δt represents the time lag. A peak at zero lag time indicates statistically coincident spiking events in different channels and therefore they should come from the same source neuron. No peak at zero lag time indicates non-coincident spiking activities and therefore they are distinct neurons. In this way, spikes that are recorded from 3 recording electrodes were identified. The average spike amplitude for each recorded neuron was defined as the average of peak-to-peak amplitudes of the spikes. Then the distances from the recording sites and the source neuron were estimated by the following fitting curve[40,56] as the recorded spike amplitudes decay

as a function of the distance from the neuron and the recording site: $V_e = \frac{-I_e R}{4\pi r}$, where V_e, I_e, R, and r stand for extracellular voltage, current, resistivity and propagation radius, respectively. The location of the identified neuron (the green circle in Fig. 3d, II) were inferred with ca. cellular resolution[41,57] by triangulating the distances from the three electrodes using several widely accepted assumptions[40].

6. Analysis of maximum stress in curved NeuE elements

6.1 Calculation of maximum stress in curved NeuE elements. From elastic beam theory for pure bending, we first determined the location of the neutral axis (NA). In the analysis below, $E_S = 2\ GPa$, $E_m = 79\ GPa$ are the Young's modulus of SU-8 and Au[16], respectively; y_{S1}, y_{S2}, y_m indicate the distance between the NA and the centroid of the top SU-8 layer, bottom SU-8 layer and Au layer, respectively; A_{S1}, A_{S2}, A_m indicate the cross-sectional area of the top SU-8 layer, bottom SU-8 layer and Au layer respectively; $b_S = 4\ \mu m$ and $b_m = 2\ \mu m$ indicate the width of SU-8 and Au, respectively; $h_S = 0.421\ \mu m$ and $h_m = 0.105\ \mu m$ indicate the thickness of SU-8 and Au, respectively; h indicates the distance between the NA with the bottom boundary of the beam; I indicates the moment of inertia; M_b indicates the bending moment; σ indicates the stress generated by the bending moment; y indicates the maximum distance from the neutral axis; κ indicates the curvature; and ρ indicates the radius of the curvature. The NA is determined from the following:

$$0 = E_m y_m A_m + E_S[(y_{S1} A_{S1}) + (y_{S2} A_{S2})]$$

$$0 = E_m(h_m/2 + h_S - h)b_m h_m + E_S[(h_m + 2h_S - h_S/2 - h) - (h - h_S/2)]b_S h_S$$

$$0 = E_m(h_m/2 + h_S - h)b_m h_m + E_S(h_m + 2h_S - 2h)b_S h_S$$

Solving this equation gives

$$h = h_m/2 + h_S$$

As noted above

$$y_{Au} = (h_m/2 + h_S - h) = 0$$

which indicates that NA lies at the center of the NeuE element.

Next, the moment of inertia (I) of the beam was calculated by the parallel axis theorem.

$$\text{I} = I_m + I_S$$

(4)

$$I_m = \frac{1}{12}b_m h_m^3 + y_m^2 A_m = \frac{1}{12} \times 2 \ \mu m \times (0.105 \mu m)^3 + 0 = 1.93 \times 10^{-4} \ \mu m^4$$

$$I_S = \left(\frac{1}{12}b_S h_S^3 + y_{S1}^2 A_{S1}\right) + \left(\frac{1}{12}b_S h_S^3 + y_{S2}^2 A_{S2}\right)$$

$$= \left(\frac{1}{12} \times 4 \ \mu m \times (0.421 \ \mu m)^3 + (0.263 \ \mu m)^2 \times 0.421 \ \mu m \times 4 \ \mu m\right) \times 2$$

$$= 0.283 \ \mu m^4$$

$$\text{I} = I_m + I_S \approx 0.283 \ \mu m^4$$

Then, the bending moment (M_b) of the beam was calculated:

$$\text{M}_b = \frac{E_m I_m + E_S I_S}{\rho} = \kappa(E_m I_m + E_S I_S)$$

(5)

The curvature is calculated based on the measurements of the 3D image data of NeuE elements. The coordinates of three points (1, 2 and 3) on a curved segment were measured, and the curvature was calculated based on the formula:

$$\kappa = \frac{4\sqrt{p(p - L_{12})(p - L_{23})(p - L_{31})}}{L_{12}L_{23}L_{31}}$$

(6)

Where L_{12}, L_{23}, L_{31} represent the distances between points 1-2, points 2-3 and points 3-1, and p indicates half the perimeter $p = \frac{L_{12}+L_{23}+L_{31}}{2}$. The maximum curvature among these measurements is $\kappa_{max} = 0.0193 \ \mu m^{-1}$, which gives the maximum bending moment $M_b = 11.2 \ pN \cdot m$.

Finally, the maximum stress (σ_{max}) in a curved NeuE ribbon from the maximum curvature that can be observed was calculated at the bottom SU-8 ribbon surface by

$$\sigma_{max} = -\frac{M_b y}{I} = -\frac{M_b \left(-\frac{h_m}{2} - h_s\right)}{I} = -\frac{11.2 \ pN \cdot m \times (-0.474 \ \mu m)}{0.283 \ \mu m^4} \approx 20 \ MPa$$

According to a previous report[39], SU-8 with a modulus of ca. 2 GPa is capable of sustaining bending stresses of up to 120 MPa before failure, which is much larger than the maximum stress in a curved NeuE element.

6.2 Simulation of maximum stress in curved NeuE elements. The bending stresses of the NeuE elements were estimated with finite element software ABAQUS as reported previously[16]. Individual electronic elements were modelled as composite shell sections with the same dimensions, layered structure, and corresponding material mechanical properties as used in **6.1**. A fixed position boundary condition was imposed on both ribbon ends, and a vertical deflection, corresponding to the maximum measured curvature with an associated deflection of $D = 8.2 \ \mu m$ was applied at the center of ribbon length. The simulated maximum bending stress of a NeuE ribbon for this deflection was 27 MPa, which is similar to that of beam model calculation and significantly below the reported failure bending stress of 120 MPa[39].

7. Replication.

The histology experiments to investigate NeuE's time-dependent interfaces with the neuronal and glial networks have been repeated on 3 independent animals for each of the Thy1-YFP-H and GFAP-GFP transgenic mouse strains at each of the four time points, resulting in 24 mice for this study. The histology experiments to investigate the smaller NeuE-2's interfaces with the neuronal network have been repeated on 2 independent Thy1-YFP-H mice. Stable single-unit recording for 12 weeks has been repeated in 3 independent mice. In addition, investigations of the migration behavior of newborn neurons has been repeated on 3 independent samples for NeuE and 20 μm control mesh at each time point, resulting in 12 mice for this study. The quantitative analyses include all of these independent samples. Last, we have also included data from 7 sham surgeries of glass capillary injections at 1 week and 2 weeks post-injection and immunohistochemical staining with GFAP/Iba-1 antibodies. In total, experiments and analyses of 48 mice were included. The number of mice used in specific experiments of the paper are summarized in Supplementary Table 2.

8. Statistics.

The variance in fluorescence intensity of all voxels within the specified distance ranges within each tissue volume was calculated, by which the combined variance and the standard error of the mean (s.e.m.) among each experimental group were determined. Comparisons between experimental groups were made using two-tailed *t*-tests assuming the variable follows a normal distribution, and *P* values of less than 0.05 were considered statistically significant.
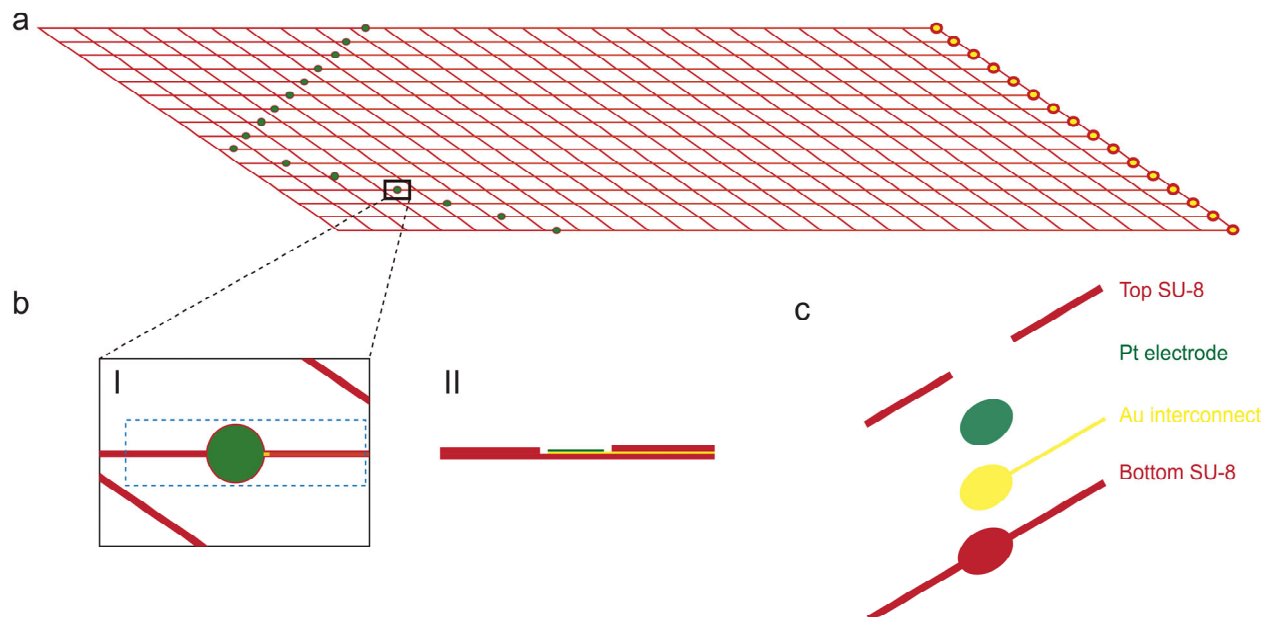
Supplementary Fig. 1 | Schematic illustration of NeuE. a, Schematics showing the overall layout of a 16-channel NeuE probe. **b**, Schematics showing the top view (I) and side view (II) of the electrode highlighted with the black box in **a**. This top view is similar to experimental micrograph (Supplementary Fig. 2a). **c**, Exploded view of the electrode highlighted within the blue dashed box in **b** showing the distinct material layers. SU-8, interconnects and electrodes are colored in red, yellow and green, respectively.
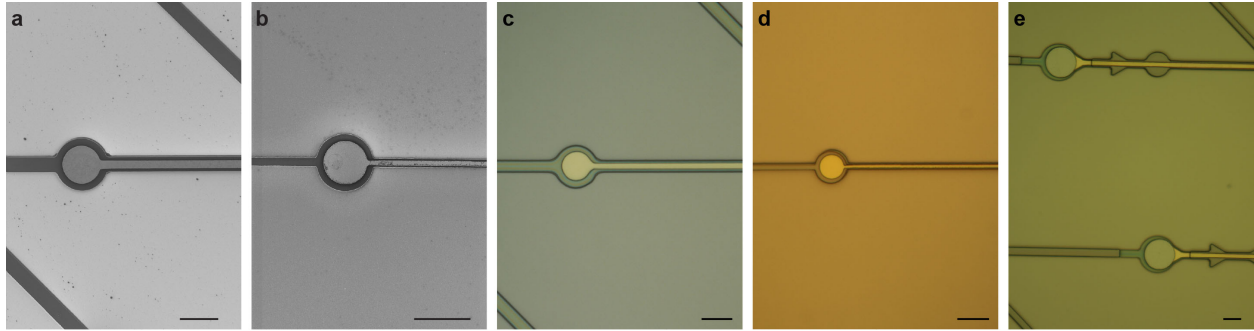
Supplementary Fig. 2 | Structural characterization of NeuE. a and **b**, Raw SEM images corresponding to Fig. 1b, II and III, respectively. **c** and **d**, Optical images showing the close-up views of the electrodes of two NeuE designs for histology. **e**, Optical image showing the close-up view of the electrodes incorporated with channel-indexing barcodes for electrophysiological recording. Scale bars, 10 μm.
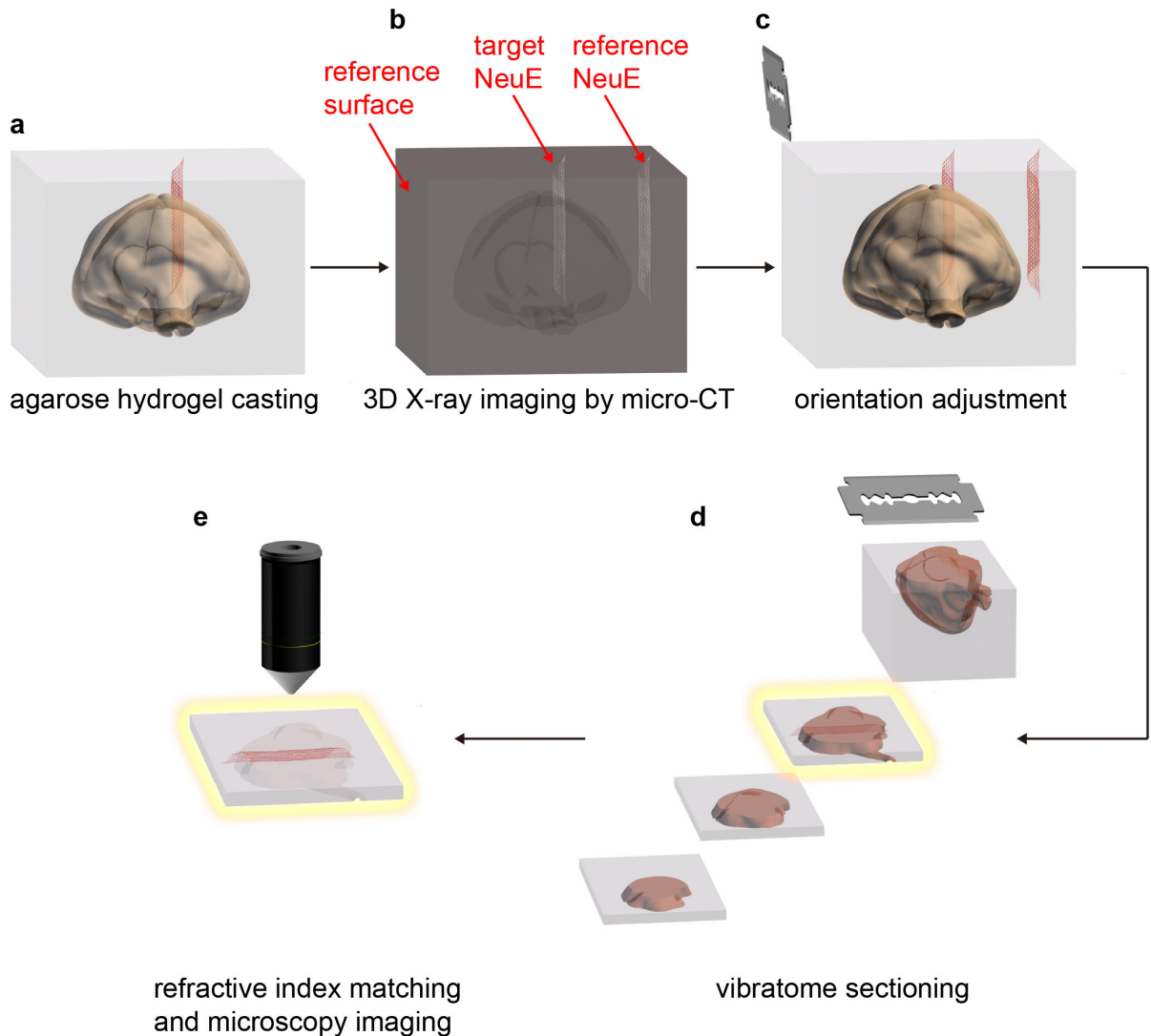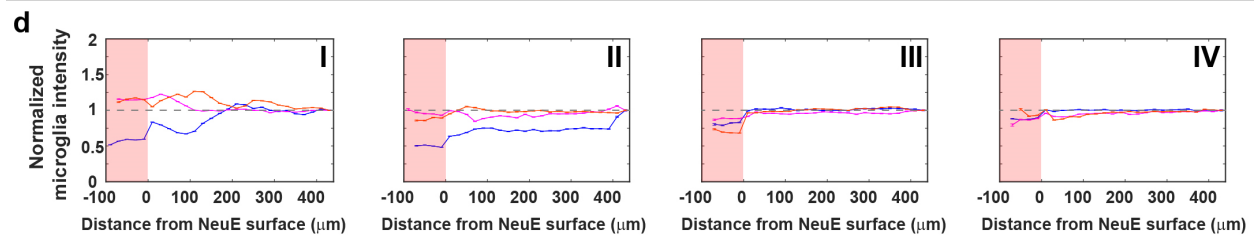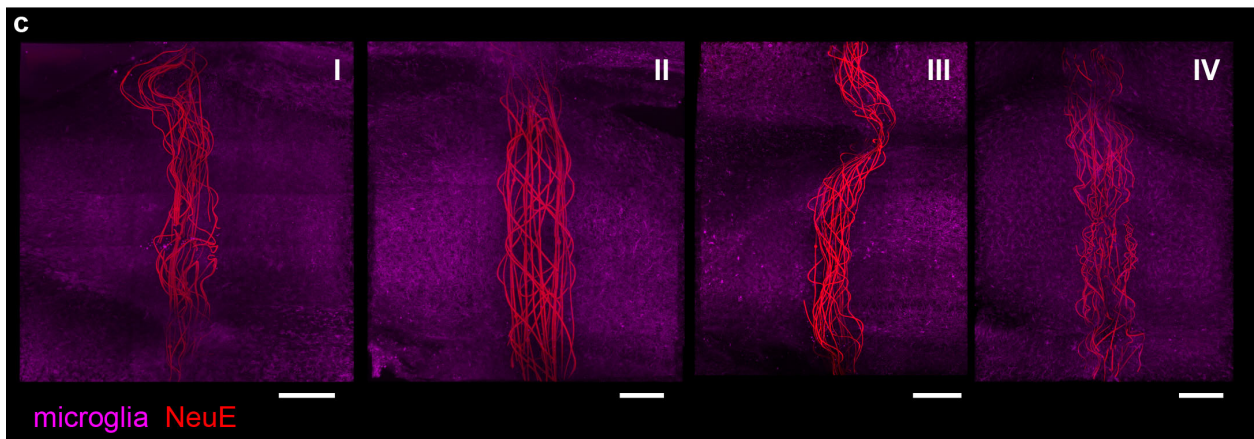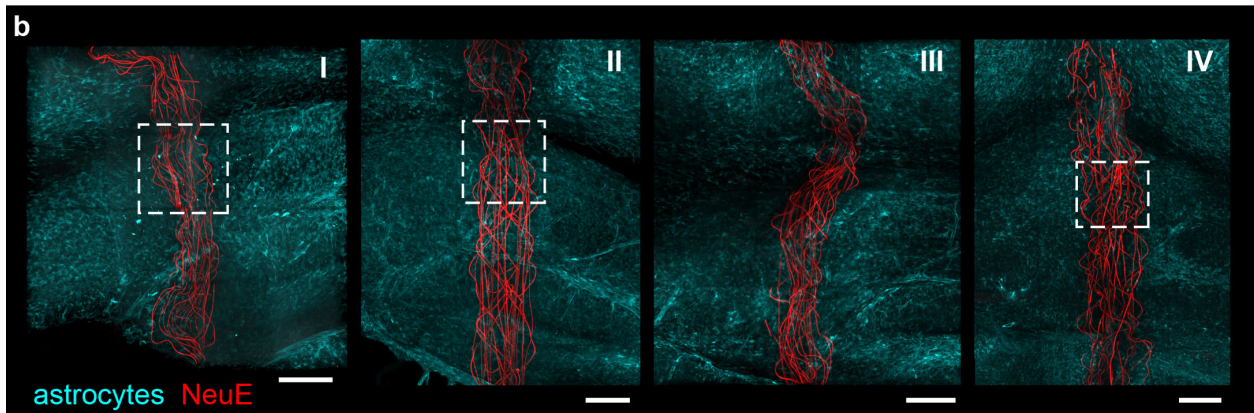
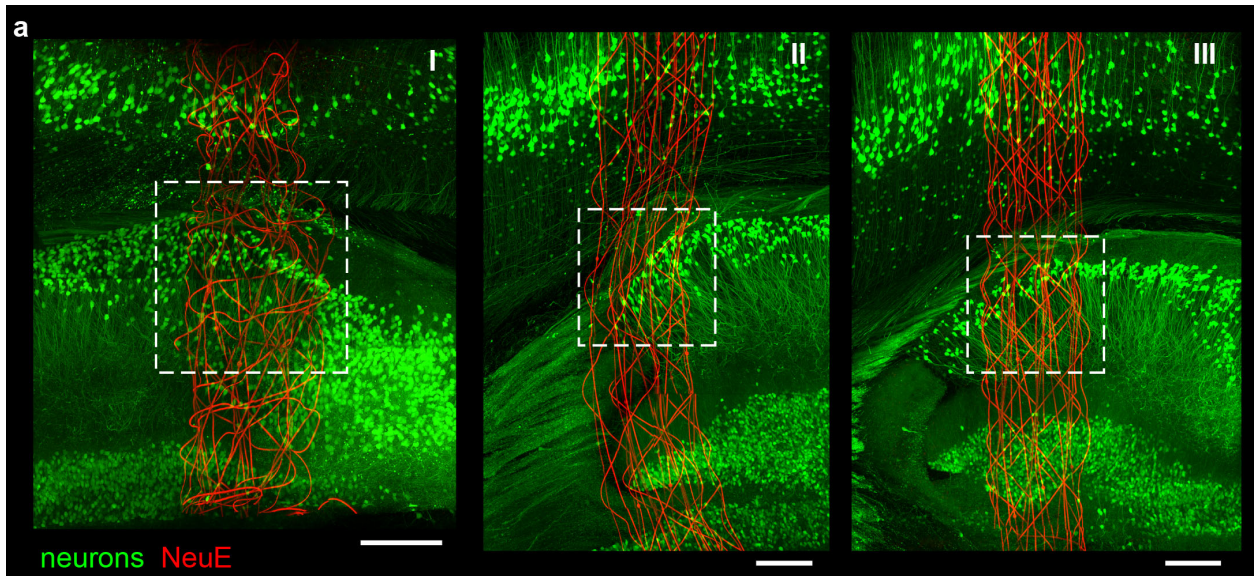**Supplementary Fig. 3 | Schematics showing key steps for 3D full probe mapping sample preparation. a**, An agarose hydrogel block containing a mouse brain with the entire injected NeuE. **b**, After a reference NeuE was injected into the hydrogel, micro-CT was used to define the location and angle of the target NeuE with respect to the reference NeuE and the reference surface, respectively. **c**, Adjustment of reference surface orientation to be parallel to the target NeuE. **d**, Vibratome sectioning to obtain the brain slice containing the full probe. The brain slice targeted for immunostaining subsequently underwent tissue clearing. **e**, The tissue was then immersed in a refractive index (RI) matching solution and imaged by confocal/two-photon fluorescence microscope.
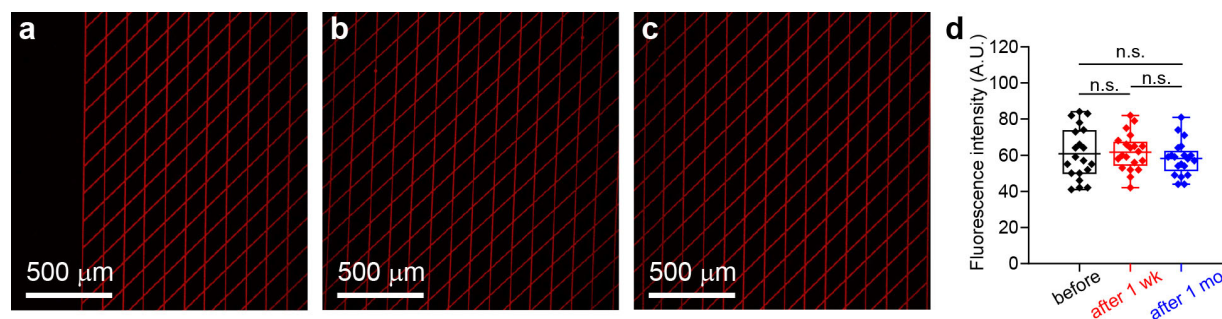
Supplementary Fig. 4 | Ex vivo characterization of fluorescence conjugation. a, Fluorescence microscope image of on-chip NeuE after device fabrication. **b** and **c**, Fluorescence microscope images of the same NeuE probe after incubation in 1× PBS at 37 °C for 1 week and 1 month, respectively. RhBen fluorescence is in red. Images were taken with maximum pinhole and the same excitation and detection parameters. Images were taken with only 3% of maximum laser power within 1 sec so that there is no photo-bleaching concern due to imaging. **d**, Box plot showing the fluorescence intensities of NeuE structures before (**a**) and after incubation in 1× PBS at 37 °C for 1 week (**b**) and 1 month (**c**) (box: 25/75 percentiles, whisker: 0/100 percentiles, and bar-in-box: mean). There is no significant difference among groups ($P = 0.83$ for before vs. after 1 wk; $P = 0.50$ for before vs. after 1 mo; $P = 0.28$ for after 1 wk vs. after 1 mo; n.s., not significant, $P > 0.05$; two-tailed t-test; N=20 independent NeuE ribbons for each condition).

a

I   II   III

neurons   NeuE

b

I   II   III   IV

astrocytes   NeuE

c

I   II   III   IV

microglia   NeuE

d

I   II   III   IV

Normalized microglia intensity

Distance from NeuE surface (μm)

Supplementary Fig. 5 | 3D full probe images of NeuE/brain interfaces. a, 3D full probe interfaces between NeuE (red) and neurons (green) at 2 days (I), 2 weeks (II) and 3 months (III) post-implantation. White dashed boxes indicate the volumes shown in Fig. 2a. Scale bars, 200 μm. **b**, 3D full probe interfaces between NeuE (red) and astrocytes (cyan) at 2 days (I), 2 weeks (II), 6 weeks (III) and 3 months (IV) post-implantation. White dashed boxes indicate the volumes shown in Fig. 2b. Scale bars, 200 μm. **c**, Iba-1 immunostaining of microglia (magenta) on the same samples shown in **b**. Scale bars, 200 μm. **d**, Normalized fluorescence intensity of microglia as a function of distance from the 3D NeuE boundary at CTX (orange), hippocampal CA1 (magenta) and DG (blue) at 2 days (I), 2 weeks (II), 6 weeks (III) and 3 months (IV) post-implantation. The pink-shaded regions indicate tissue volumes within the interior of the NeuE. The relative signal was obtained by normalizing the fluorescence intensity with the baseline value defined as the fluorescence intensity averaged remote to the probe (gray dashed horizontal lines; Supplementary Note 4). The microglia distribution at the surface of the probes is 96% ± 13% (mean ± s.d.) of baseline, and remains uniform through CTX, CA1 and DG brain regions over this extended time period. All error bars reflect ±1 s.e.m. Time-dependent 3D histology data have been collected and analyzed for N=3 independent samples for neurons and astrocytes and N=1 sample for microglia at each time point, totaling N=12 independent samples each for neurons and astrocytes and N=4 samples for microglia.
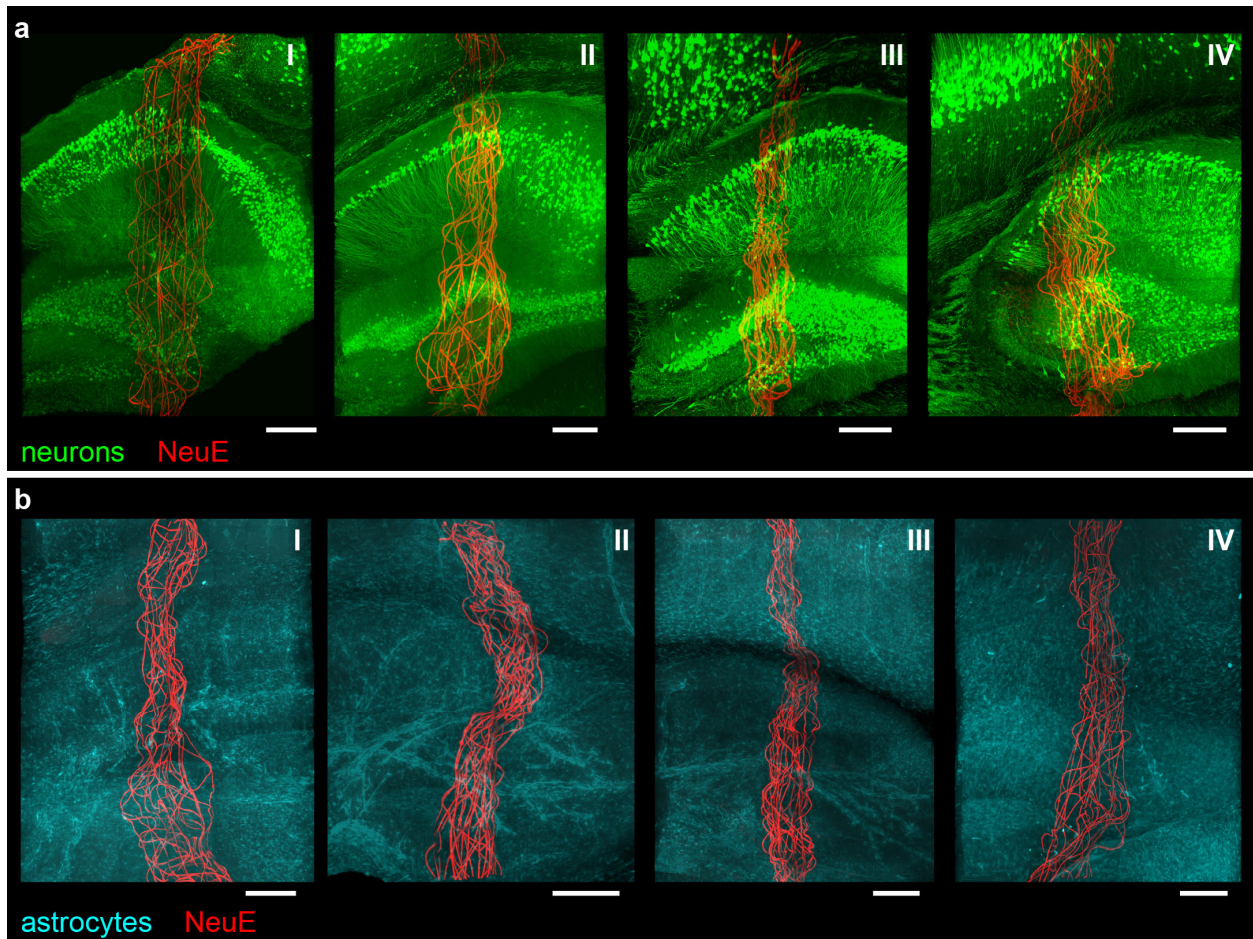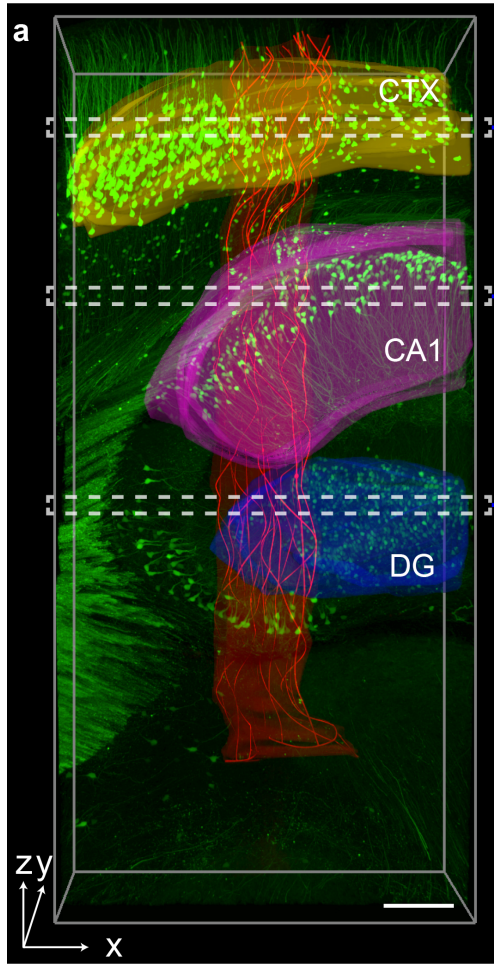
Supplementary Fig. 6 | Independent replicates of time-dependent 3D histology studies of NeuE/brain interfaces. a, 3D full probe interfaces between NeuE (red) and neurons (green) at 2 days (I), 2 weeks (II), 6 weeks (III) and 3 months (IV) post-implantation. Parts of the tissue in the cortex were damaged during sample handling and were excluded from analysis. The undamaged parts of the cortex (right part for I, left parts for II-IV) were analyzed. Scale bars, 200 μm. **b**, 3D full probe interfaces between NeuE (red) and astrocytes (cyan) at 2 days (I), 2 weeks (II), 6 weeks (III) and 3 months (IV) post-implantation. Scale bars, 200 μm. Time-dependent 3D mapping has been repeated on N=3 independent samples for each time point on each transgenic mouse strain, with additional data and analyses shown in Figs. 1-2 and Supplementary Figs. 5 and 7.
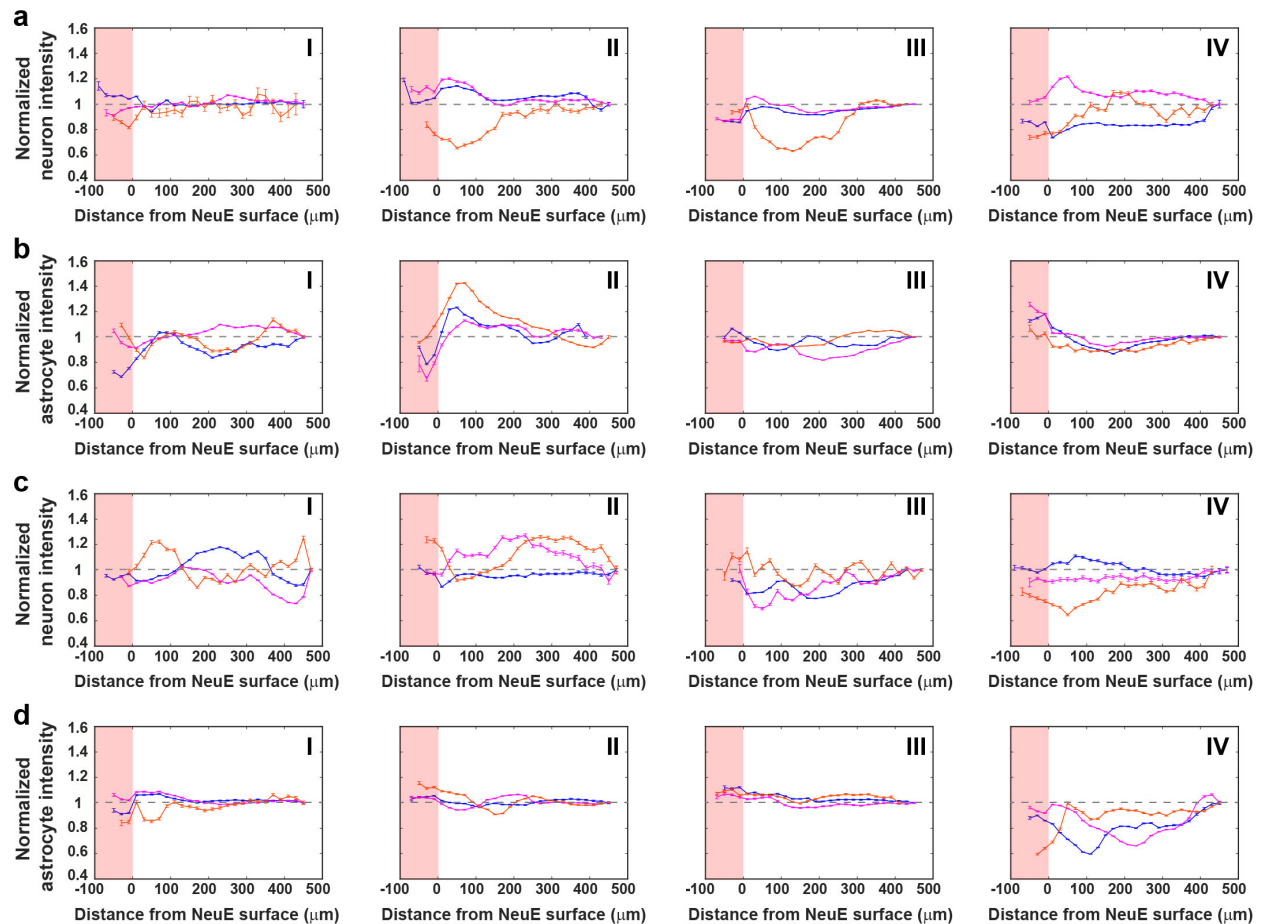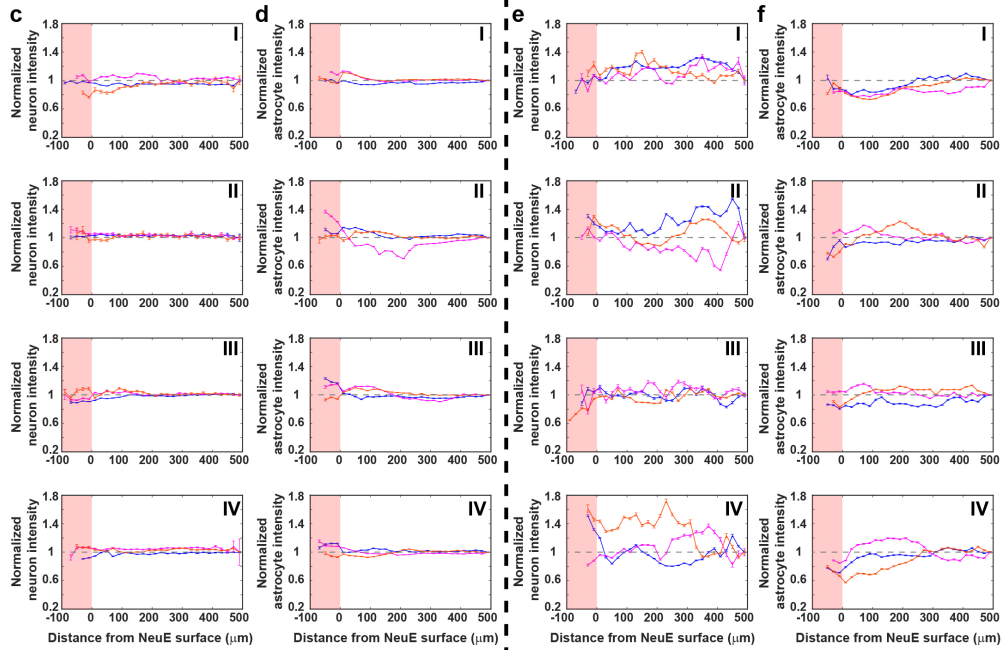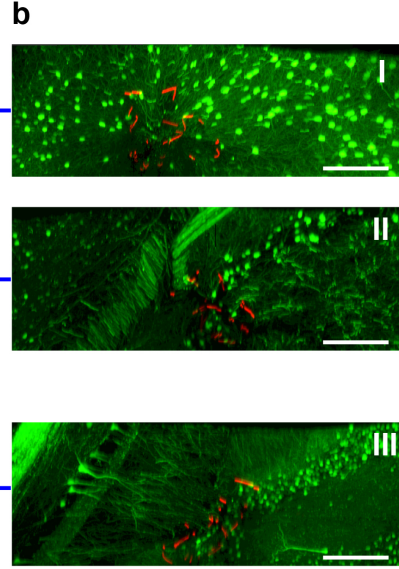
Supplementary Fig. 7 | Quantitative analysis of time-dependent 3D histology independent replicates. a and **b**, Normalized fluorescence intensity of neurons (**a**) and astrocytes (**b**) as a function of distance from the 3D NeuE boundary at CTX (orange), hippocampal CA1 (magenta) and DG (blue) at 2 days (I), 2 weeks (II), 6 weeks (III) and 3 months (IV) post-implantation. The pink-shaded regions indicate tissue volumes within the interior of the NeuE. The relative signal was obtained by normalizing the fluorescence intensity with the baseline value defined as the fluorescence intensity averaged remote to the probe (gray dashed horizontal lines; Supplementary Note 4). All error bars reflect ±1 s.e.m. **c** and **d**, Normalized fluorescence intensity of neurons (**c**) and astrocytes (**d**) as a function of distance from the 3D NeuE boundary at CTX (orange), hippocampal CA1 (magenta) and DG (blue) at 2 days (I), 2 weeks (II), 6 weeks (III) and 3 months (IV) post-implantation from another independent set of cohorts (Supplementary Note 4). All error bars reflect ±1 s.e.m. Time-dependent 3D histology studies and quantitative analyses have been repeated on N=3 independent samples, with additional data and analyses shown in Figs 1-2 and Supplementary Figs. 5-6. These analyses show neuron interpenetration inside NeuE and minimal

astrocyte increases at the surface and interior of NeuE at all time points, and thus demonstrate the reproducibility of these results.

Histology on 3D volumes

Histology on 2D horizontal slices

a

CTX

CA1

DG

z y

x

b

I

II

III

c

Normalized neuron intensity

I

II

III

IV

Distance from NeuE surface (μm)

d

Normalized astrocyte intensity

I

II

III

IV

Distance from NeuE surface (μm)

e

Normalized neuron intensity

I

II

III

IV

Distance from NeuE surface (μm)

f

Normalized astrocyte intensity

I

II

III

IV

Distance from NeuE surface (μm)

21

**Supplementary Fig. 8 | Illustration and comparison of 3D volumes and 2D horizontal sections. a**, 6×15 tiles in x-z plane with a series of ca. 1000 0.5-µm-thick slices per tile along y direction together produce a 3D visualization of the NeuE in contact with a volume of tissue spanning from the cortex (orange shade) through the CA1 (magenta shade) and the DG (blue shade) corresponding to the typical regions analyzed in these studies. Scale bar, 200 µm. **b**, Horizontal sections with a thickness of 50 µm are shown from each of cortex (I), CA1 (II) and DG (III) regions indicated by the dotted lines. The 3D visualization allows us to quantify the fluorescence intensity from the entirety of the desired brain region, whereas the 2D slices represent only a small subset of these data, and thus the quantification of fluorescence in 3D represents a more thorough comparison for the fluorescence near the probe and away from the probe in a given brain region. Scale bars, 200 µm. **c** and **d**, Normalized fluorescence intensity of neurons (**c**) and astrocytes (**d**) as a function of distance from the 3D NeuE boundary at CTX (orange), hippocampal CA1 (magenta) and DG (blue) at different time points analyzed on the thick sections, same as Fig. 2c,d. **e** and **f**, Normalized fluorescence intensity of neurons (**e**) and astrocytes (**f**) analyzed on the 50 µm horizontal slices. The pink-shaded regions indicate tissue volumes within the interior of the NeuE. The relative signal was obtained by normalizing the fluorescence intensity with the baseline value defined as the fluorescence intensity averaged over a range of 480-500 µm away (gray dashed horizontal lines; Supplementary Note 4). All error bars reflect ±1 s.e.m. The analysis of cell distribution in regions of the 3D volume shows the same overall trend as the analysis of the horizontal slices but with significantly less fluctuation in the fluorescence intensity. Comparison of the normalized fluorescence intensity from tissue volumes versus thin horizontal slices relative to the NeuE probes for both neurons and astrocytes show similar overall results on a total of 24 tissue sections; that is, no evidence for suppression of neuron density or proliferation of astrocytes near the probe from day-2 to 90 post-implantation, although there are substantially smaller fluctuations in the fluorescence intensities analyzed on the 3D volume samples. The smaller fluctuations can be attributed to the much larger number of cells contained within the 3D volume samples, which contain most of those cells in each of the distinct DG, CA1 and CTX brain regions, whereas conventional horizontal slices can fluctuate depending on the specific location of the slice within the brain region and corresponding cell distribution.
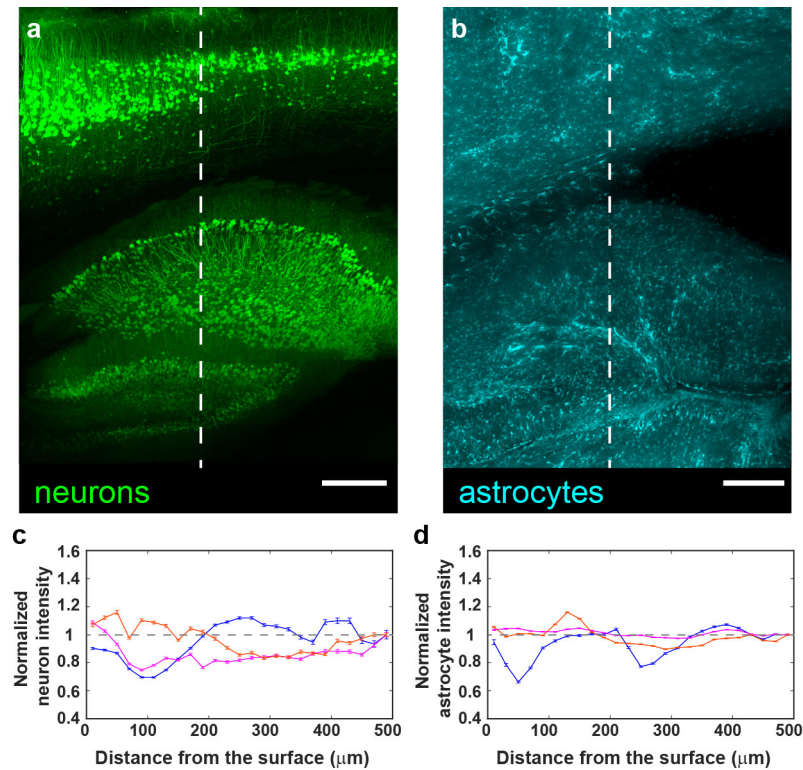
Supplementary Fig. 9 | Fluorescence images and quantitative analyses for Thy1-YFP-H and GFAP-GFP transgenic mouse tissue samples without implantation. a and **b**, distributions of neurons (**a**, green) and astrocytes (**b**, cyan) without implantation. The arbitrary vertical white dashed lines indicate the proxy for the probe that serve as references for fluorescence intensity analysis. Scale bars, 200 μm. **c** and **d**, Normalized fluorescence intensity of neurons (**c**) and astrocytes (**d**) relative to the baseline value (gray dashed horizontal lines) as a function of distance from the assumed probe at CTX (orange), hippocampal CA1 (magenta) and DG (blue), respectively (Supplementary Note 4). All error bars reflect ±1 s.e.m. These results for three brain regions from one individual mouse each for neurons and astrocytes are similar to samples of the same brain regions with NeuE implantation.
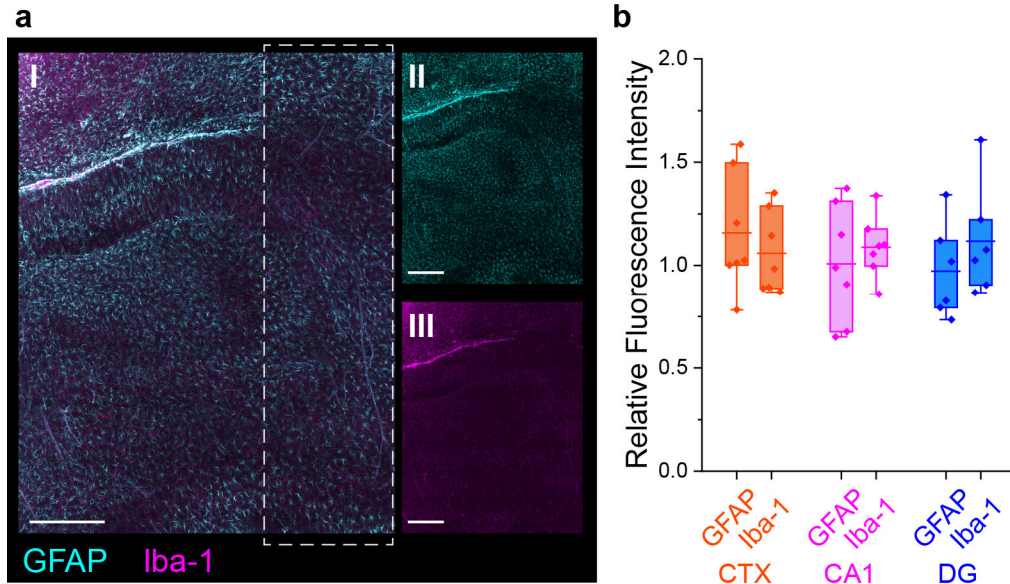
Supplementary Fig. 10 | Histological assessment of sham surgeries. Sham needle insertion/fluid injection in the HIP-to-CTX with similar PBS volumes but no NeuE probes, similar to injections with NeuE. The brain tissues containing the sham injection were collected at 1 week and 2 weeks post-injection, cleared and stained with GFAP and Iba-1 antibodies for astrocytes and microglia, respectively (Methods). **a**, Panels I, II and III display the composite, GFAP and Iba-1 images, respectively, from a representative sample at 1 week post sham injection. The white dashed box indicates the sham injection site. Scale bars, 400 μm. **b**, Box plot showing relative fluorescence intensity within the needle insertion track normalized against baseline values at 340-440 μm away from the injection site (box: 25/75 percentiles, whisker: 0/100 percentiles, and bar-in-box: mean; Supplementary Note 4). N=7 independent samples for CTX and CA1 and N=6 independent samples for DG (DG of one sample was damaged during tissue preparation). These fluorescence images and quantitative analyses show minimal immune response as revealed by ca. endogenous levels of astrocytes and microglia post sham injection. These results are consistent with previous studies[47,58] that reported injections into neural tissue using capillary needles, which are widely adopted for delivering biological species to the brain, have minimal immune response.
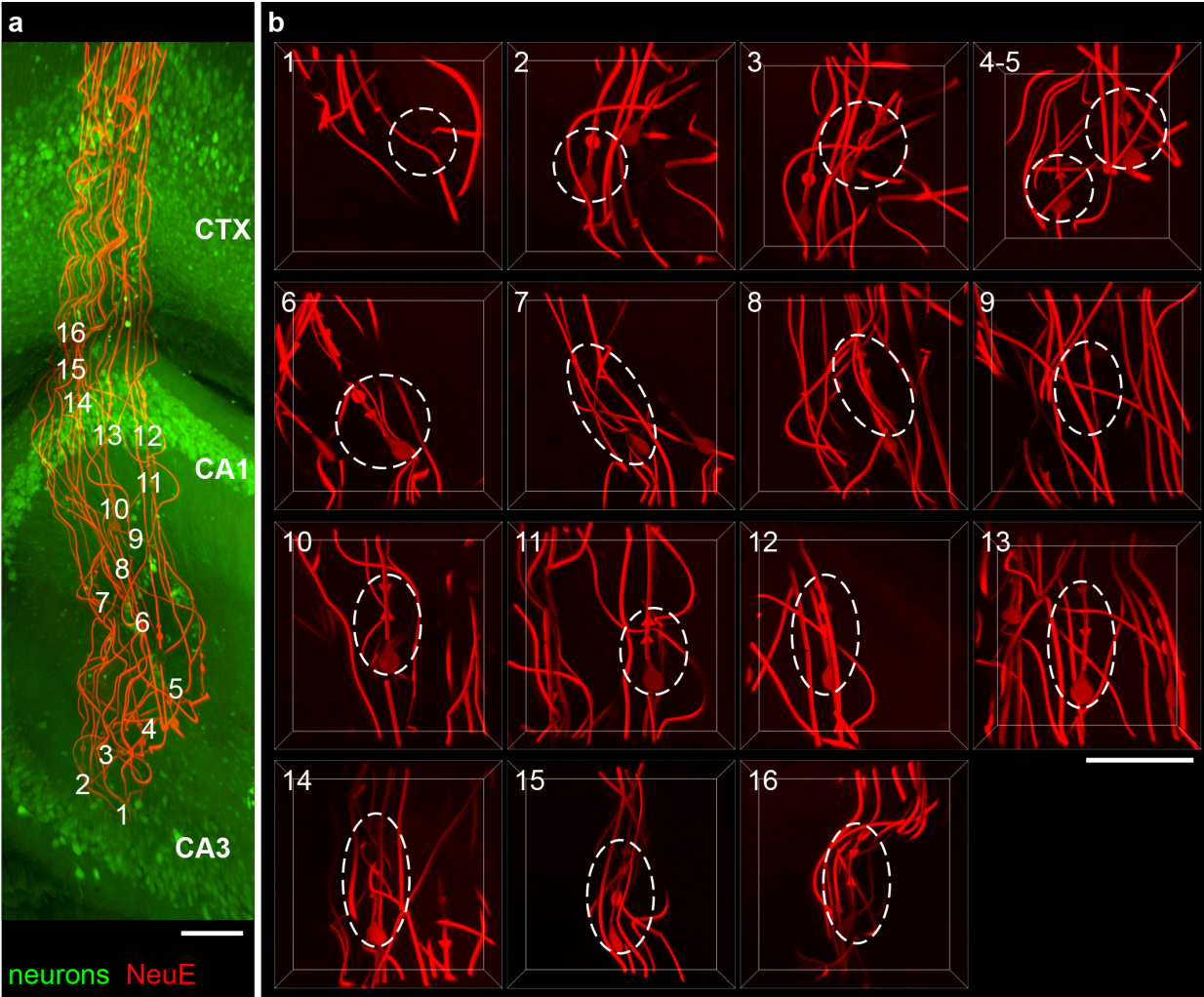
Supplementary Fig. 11 | 3D images of full NeuE/brain interface for chronic recording and channel barcodes. a, 3D NeuE/brain interface at the chronic recording endpoint of day 90. The locations of the numbers indicate the locations of electrodes with corresponding channel indices. Scale bar, 100 μm. **b**, High-resolution images of 16 barcoded electrodes, with white dashed circles highlighting electrodes and associated triangle/circle barcodes (except for electrode 1). Note that electrode 1 is ca. perpendicular to the imaging direction. Scale bar, 100 μm. The positions of all the barcoded electrodes (N=16) can be independently resolved by 3D mapping. It is possible to resolve the NeuE electrodes in all imaged samples including those without barcodes (33 samples), but the barcodes are necessary to index the channels.
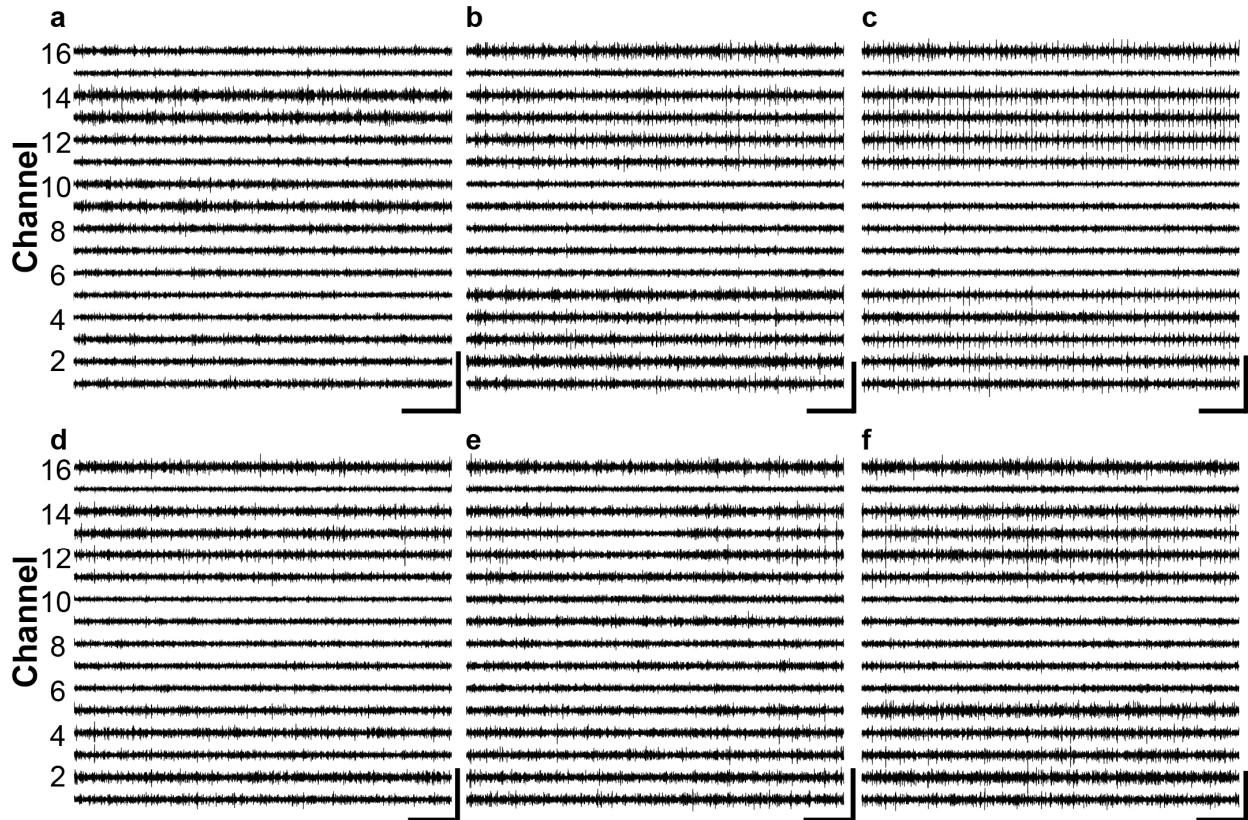
Supplementary Fig. 12 | Chronic electrophysiological recording. Representative 16-channel single-unit spike traces from the same mouse in Fig. 3a at days 0 (**a**), 14 (**b**), 26 (**c**), 40 (**d**), 66 (**e**) and 90 (**f**) post-injection. The x- and y-axes represent recording time and voltage. Scale bars, 100 ms (horizontal) and 100 µV (vertical). These data were collected for N=3 independent mice over 3 months.
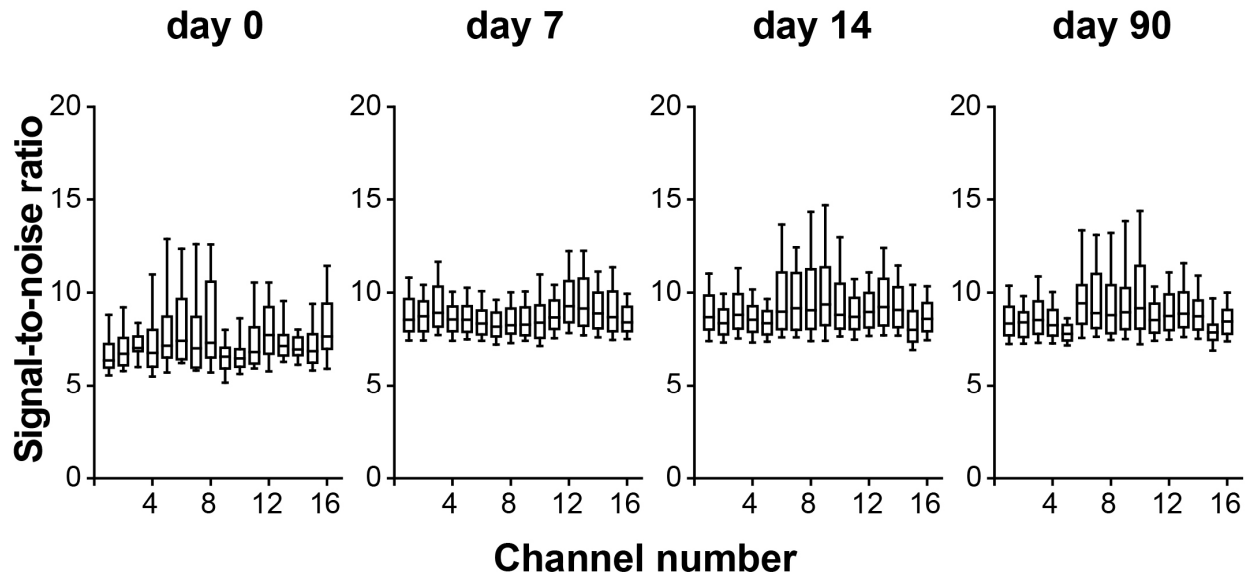
Supplementary Fig. 13 | Box plots showing the signal-to-noise ratios from all channels at days 0, 7, 14 and 90 post-injection from the same mouse in Fig. 3. Box: 25/75 percentiles, whisker: 10/90 percentiles, and bar-in-box: median. The single-unit spike signal-to-noise ratios show nearly constant values from 7.6 ± 0.6 (mean $\pm$ s.d.) at day 0 to 9.0 ± 0.5 at days 7-90 computed based on an average of ca. 250 spikes per channel.
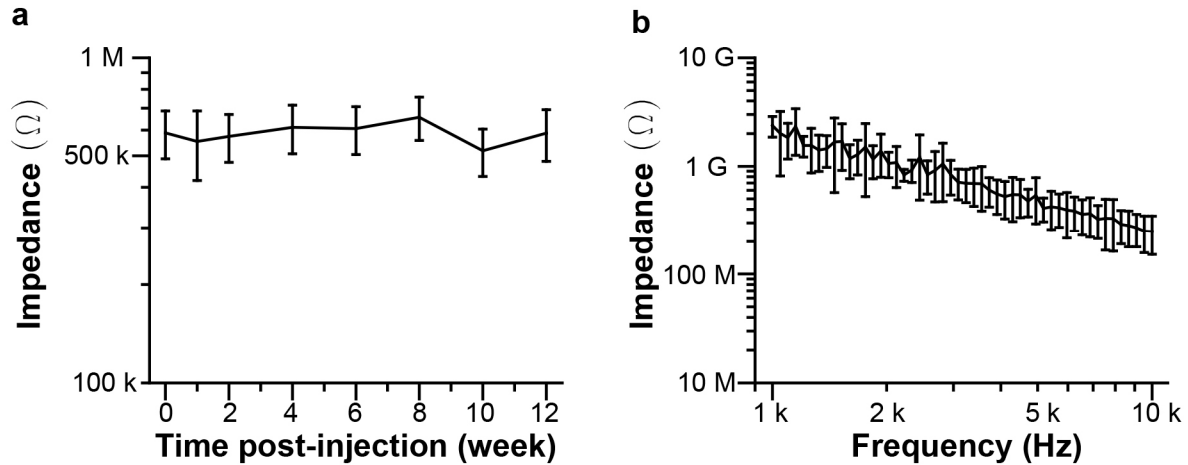
Supplementary Fig. 14 | Electrode and inter-channel impedance characterization of NeuE.
a, Time-dependent average electrode interfacial impedance at 1 kHz measured by the Intan system. The averages were obtained over 16 platinum electrodes. Error bars represent ± s.d. The electrode interfacial impedances exhibited relatively constant values of 0.6 ± 0.1 MΩ (mean ± s.d.) at days 0 and 90. **b**, Average impedance values between adjacent metal interconnects measured in the frequency range of 1 kHz to 10 kHz. The averages were obtained over 8 pairs of adjacent metal interconnects. Error bars represent ± s.d. The inter-channel impedances (order of 1 GΩ) were three orders of magnitude larger than the electrode impedances (order of 0.6 MΩ) at the 1-3 kHz relevant frequency of single-unit action potentials, and thus indicate there is minimal electrical crosstalk.
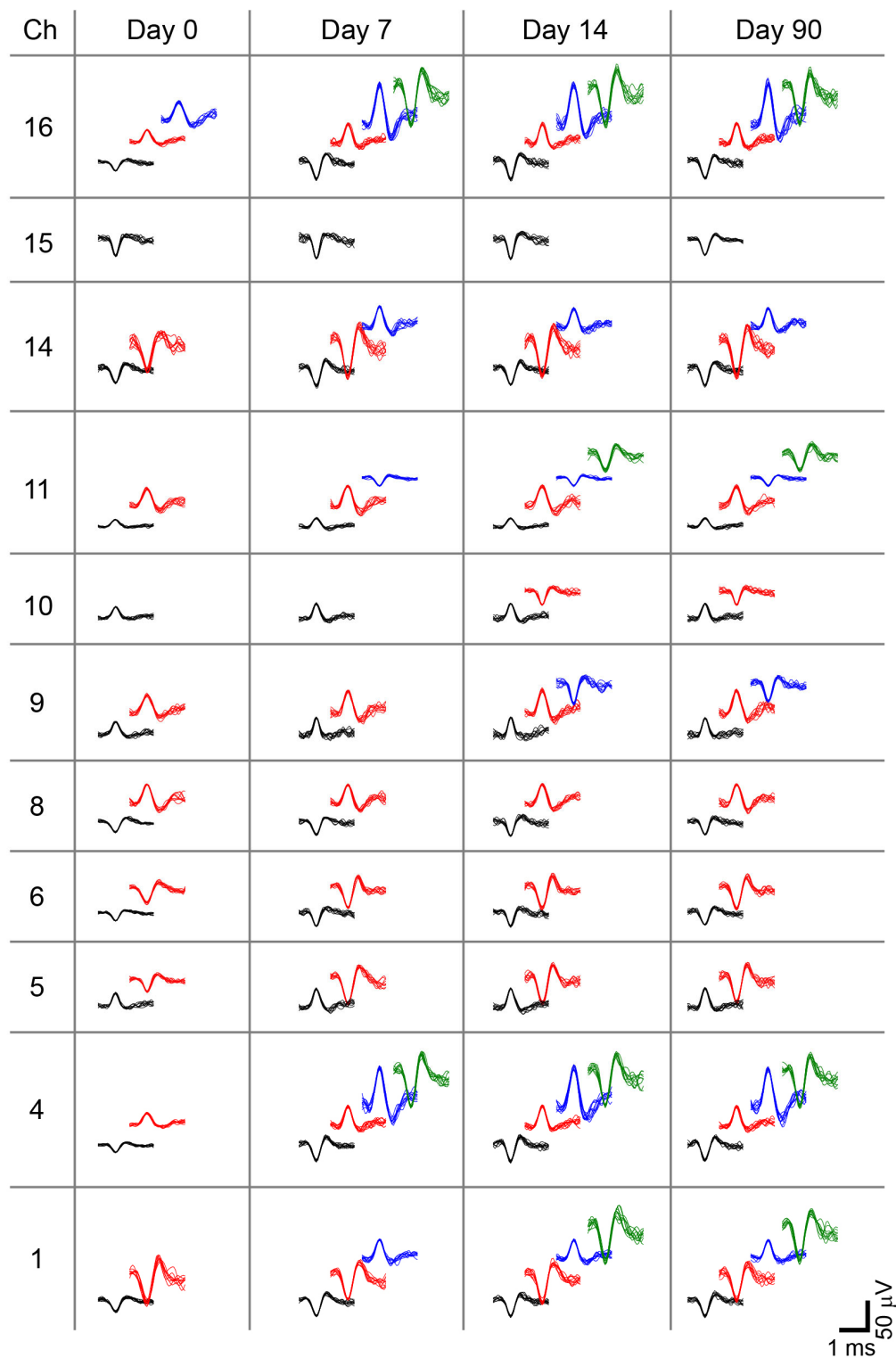
Supplementary Fig. 15 | PCA-clustered spikes of all the other channels not shown in Fig. 3b.
For each channel, each distinct color represents a unique identified neuron.
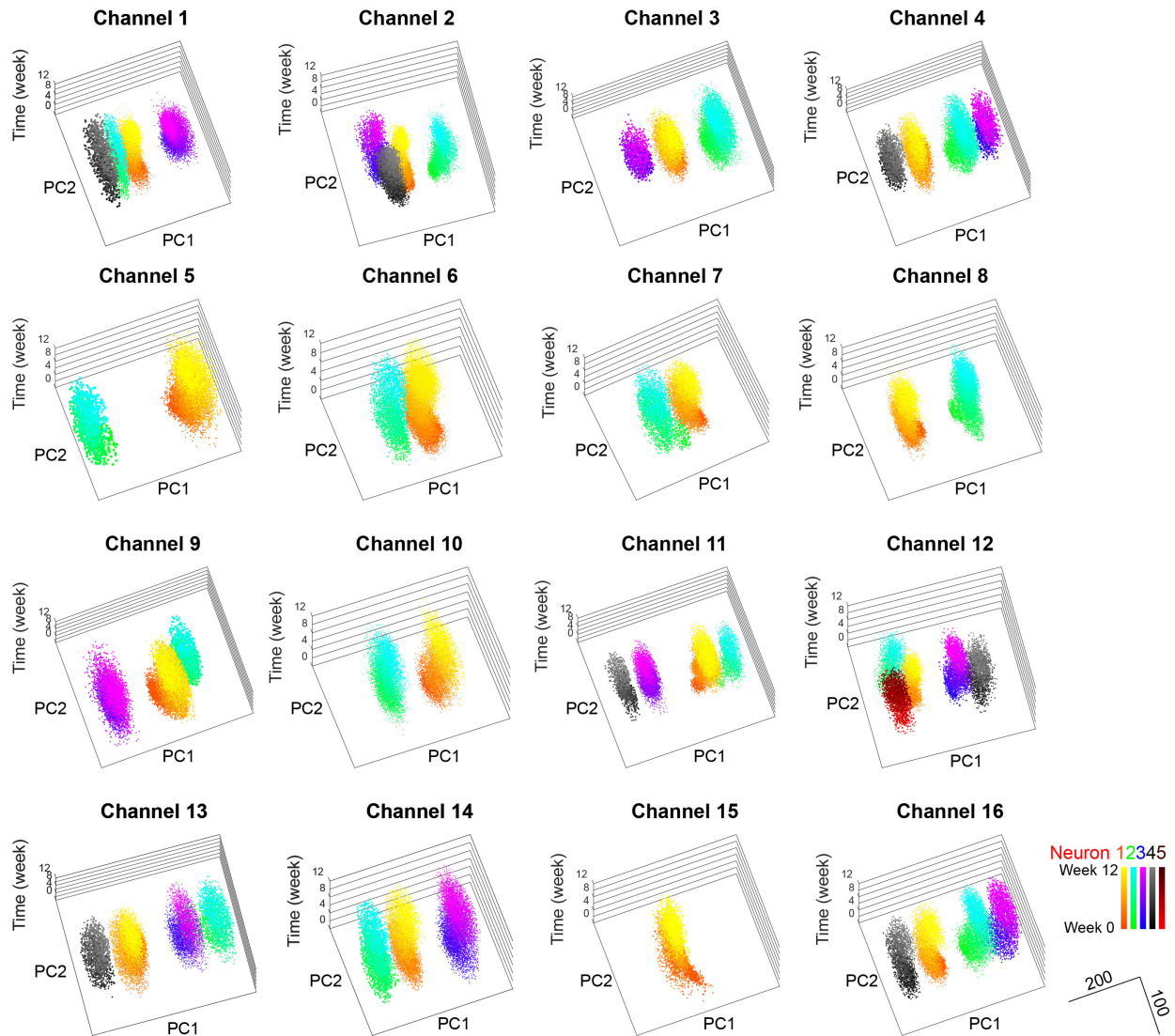
Supplementary Fig. 16 | Time evolution of single-unit spikes of all the 16 channels shown in Fig. 3 clustered by PCA at N=8 time points (weeks 0, 1, 2, 4, 6, 8, 10 and 12). The x- and y-axes denote the first and second principal components, respectively, and the z-axes indicate post-injection time. Each gradient color-coded cluster represents a distinct neuron for each channel. The color bars show the corresponding post-injection time points from 0 to 12 weeks of the 3D PCA plots. These data show stable clusters with nearly constant positions in the first and second principal component plane (PC1-PC2) over the entire recording period.
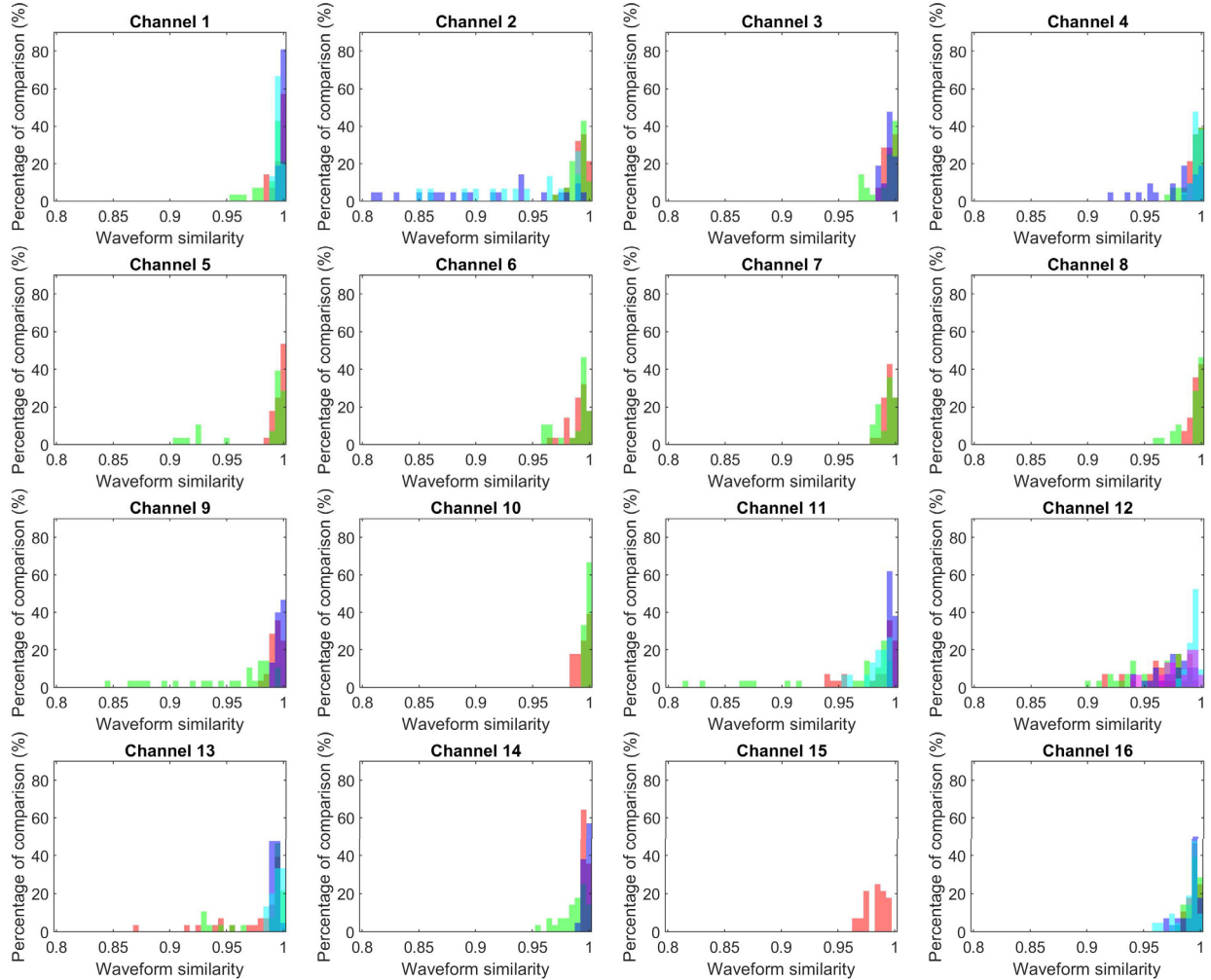
Supplementary Fig. 17 | Cross-day auto-correlation analyses of average spike waveforms across 3 months. Autocorrelation histograms of average waveforms for each of the identified clusters (color-coded in red, green, blue, cyan and magenta for neurons 1 to 5, respectively) for the same mouse shown in Fig. 3 at 8 time points (weeks 0, 1, 2, 4, 6, 8, 10 and 12). The colors are rendered with the transparency of 50% to make all of the overlapped bars visible. The values of waveform similarity nearing 1 indicate that the waveforms are stable throughout the 3-month recording period. Specifically, 100% of waveform similarity r values are > 0.80, 97.7% of r values are > 0.90 and 92.7% of r values are > 0.95.
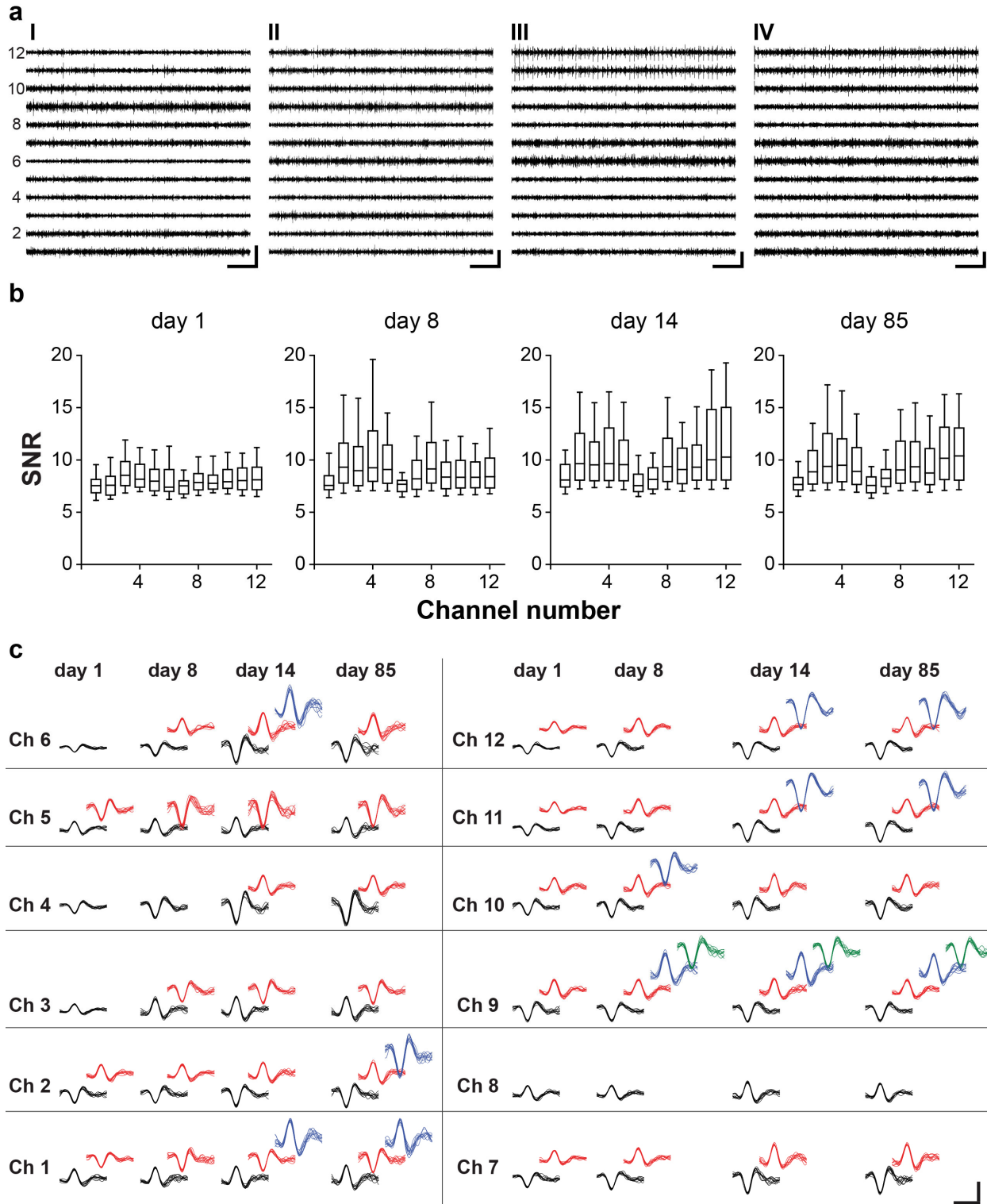
Supplementary Fig. 18 | Single-unit stability characterization of Mouse 2. **a**, Representative single-unit spike traces at days 1, 8, 14 and 85 post-injection, exhibiting stable single-unit spikes from day 1 to 85, the measurement endpoint. The x- and y-axes represent recording time and

voltage. Scale bars, 100 ms (horizontal) and 50 µV (vertical). **b**, Box plots showing the SNR from all channels at days 1, 8, 14 and 85 post-injection (box: 25/75 percentiles, whisker: 10/90 percentiles, and bar-in-box: median). SNRs for all channels (computed based on an average of ca. 230 spikes per channel) are stable over time with an average of 7.4% cross-time variation. **c**, Time evolution of spikes of PCA-clustered single-units from all channels over 3 months post-injection. For each channel, each distinct color in the sorted spikes represents a unique identified neuron. Scale bars, 1 ms (horizontal) and 50 µV (vertical). The isolated neurons are stable over the three months of recording without evidence of changes in waveform. Note that 12 out of 16 channels were connected at the input-output interface following implantation, and all of the initially connected channels remained functional throughout the entire experiment.
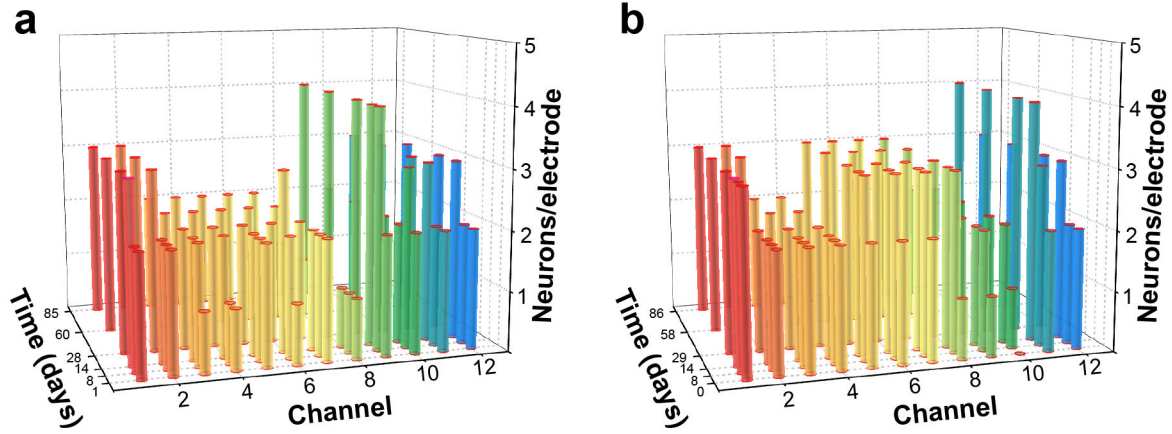
Supplementary Fig. 19 | 3D bar charts of the number of distinct neurons recorded per electrode as a function of the time post-injection of Mouse 2 (a) and Mouse 3 (b). These data show an increase in the number of neurons/electrode over the first 2 weeks in 16 out of 24 channels, followed by no change for the remainder of the experiment, except for 2 channels with an increase of 1 neuron and 1 channel with a decrease of 1 neuron. These data are consistent with the probe in the main text with a total of 40 initially connected channels among the 3 mice, and emphasize the reproducibility of both the initial increase in neurons/electrode over the first 2 weeks as well as the stability of neurons/electrode throughout the rest of the experiment.
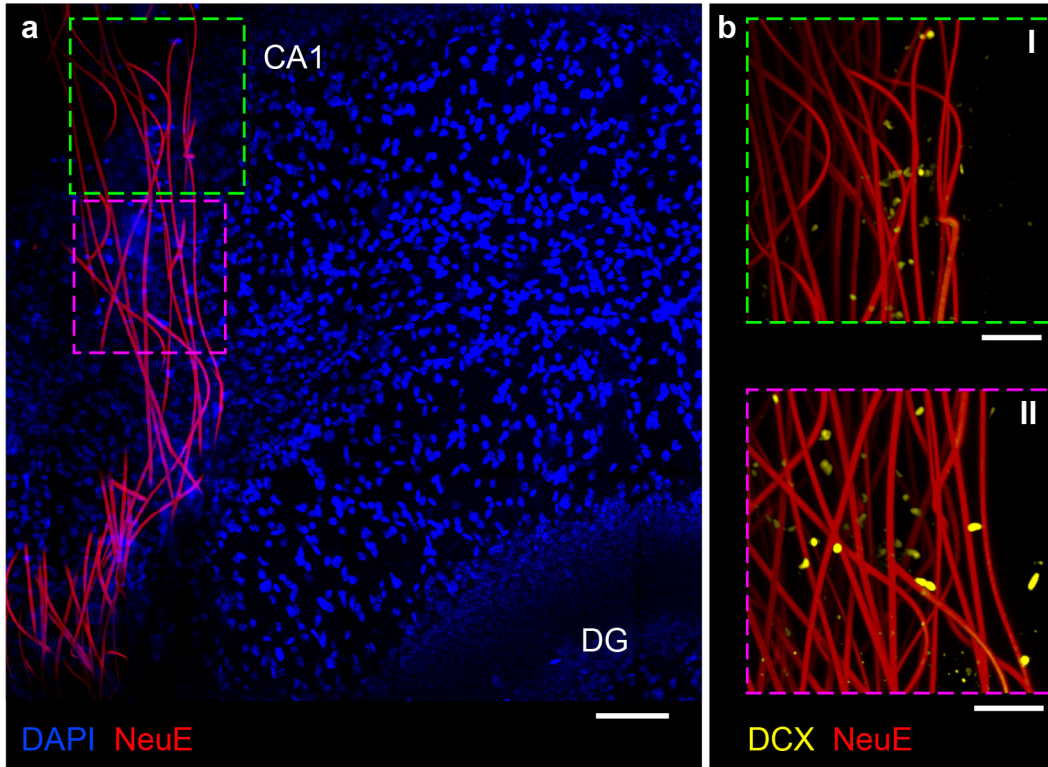
Supplementary Fig. 20 | Global and zoomed-in images of NeuE/brain interfaces at 2 weeks post-injection. a, A 50-μm thick section within the optically reconstructed volume showing the position of NeuE relative to HIP CA1 and DG. Scale bar, 100 μm. **b**, High-resolution 3D images of the volumes highlighted by the green and magenta dashed boxes in **a**. Scale bars, 50 μm. NeuE (red); DAPI (blue); DCX (yellow). This experiment has been repeated on N=3 independent samples and quantitatively summarized in Fig. 4c.
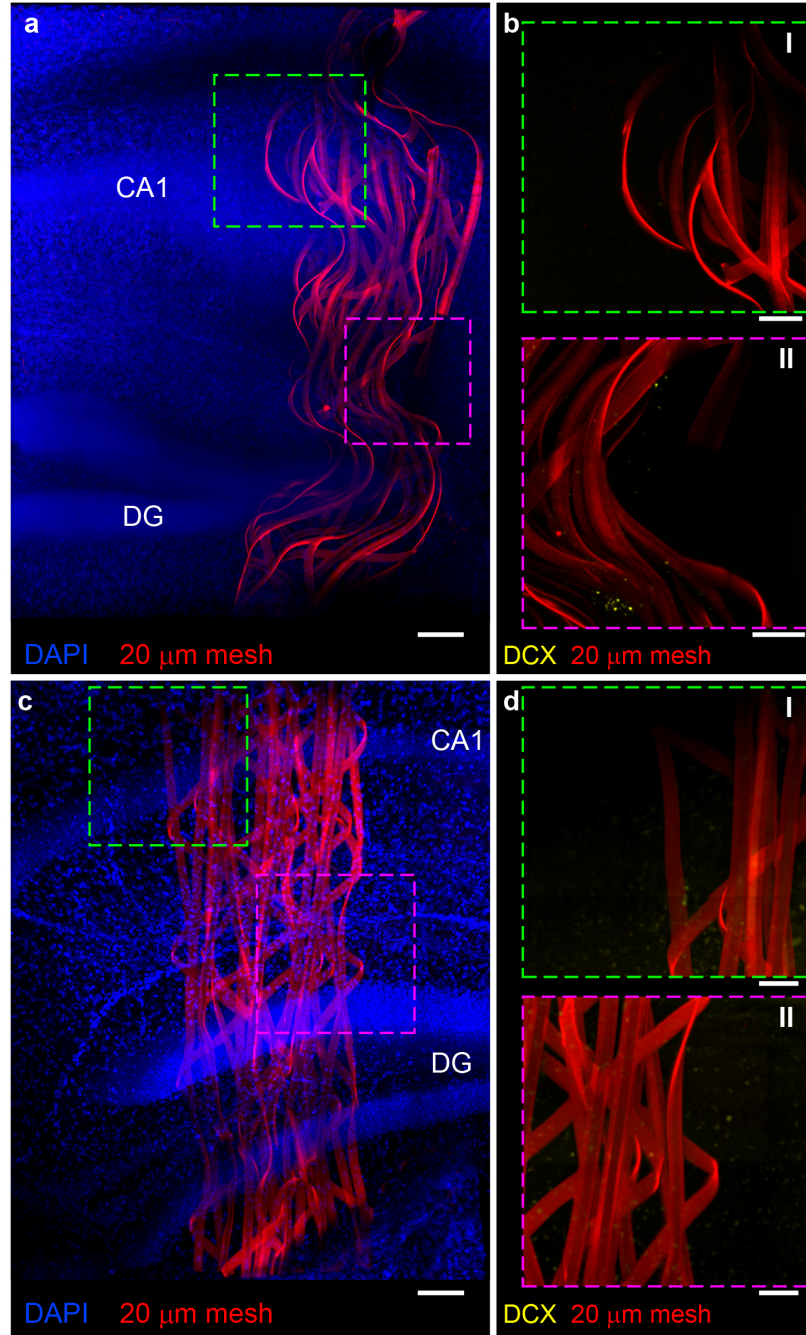
Supplementary Fig. 21 | 3D brain interface of control injections with 20 μm mesh. a and **c**, 3D images of tissue samples at 1 week (**a**) and 2 weeks (**c**) post-injection, with DAPI in blue and 20 μm mesh in red. Scale bars, 100 μm. **b** and **d**, High-resolution images of green and magenta dashed box areas in **a** and **c**, respectively, with DCX in yellow and 20 μm mesh in red. Scale bars, 50 μm. Each condition has been repeated on N=3 independent samples and quantitatively summarized in Fig. 4c.

Supplementary Table 1 | Structural parameters of NeuE probes.

NeuE design	Total width W (mm)	SU-8 width w (μm)	Metal interconnect width w_m (μm)	Angle between longitudinal and transverse SU-8	Unit cell (μm × μm)	Diameter of electrodes (μm)	2D porosity	3D porosity
NeuE-1	2	4	2	45°	333 × 125	10 or 20	95.64%	99.73%
NeuE-2	2	1	0.6	45°	333 × 125	8	98.90%	99.93%

Supplementary Table 2 | Summary of replicate experiments in these studies.

Experiment	Number of replicates	Total number of samples
NeuE histology for neuronal integration	3	12
NeuE histology for astrocyte distribution	3	12
NeuE histology for microglia distribution	1	4
NeuE-2 histology for neuronal integration	2	2
NeuE electrophysiology	3	3
NeuE histology for migration of newborn neurons	3	6
Control mesh histology for migration of newborn neurons	3	6
Sham injection histology for astrocyte and microglia distributions	3 and 4	7
Total number of independent samples (after subtracting the overlapped samples used for multiple experiments): 48		

Supplementary Table 3 | L-ratio on days 0, 7, 14 and 90 post-injection for each identified neuron in all channels of a representative NeuE probe presented in Fig. 3. This analysis provides a statistical measure of how well separated the spikes of one cluster (putative neuron) are from other spikes recorded simultaneously on the same electrode (Supplementary Note 5)[37,38]. An L-ratio of < 0.05 of a specific isolated unit among all sorted spikes is considered good separation/isolation[37,38]. N/A indicates not applicable for the channels that only one neuron is identified.

Channel	Neuron(s), L-ratio(s)			
	Day 0	Day 7	Day 14	Day 90
1	N1, 1.08×10^{-3}; N2, 4.14×10^{-3}	N1, 3.16×10^{-3}; N2, 1.18×10^{-2}; N3, 2.29×10^{-6}	N1, 1.87×10^{-2}; N2, 5.92×10^{-4}; N3, $<1\times10^{-6}$; N4, 3.24×10^{-3}	N1, 5.49×10^{-3}; N2, 5.78×10^{-5}; N3, $<1\times10^{-6}$; N4, 2.33×10^{-2}
2	N1, 1.26×10^{-4}; N2, 4.07×10^{-3}	N1, 7.51×10^{-4}; N2, $<1\times10^{-6}$; N3, 1.81×10^{-2}	N1, 4.67×10^{-4}; N2, $<1\times10^{-6}$; N3, 2.14×10^{-3}; N4, 3.55×10^{-3}	N1, 8.29×10^{-3}; N2, $<1\times10^{-6}$; N3, 6.31×10^{-3}; N4, 3.78×10^{-2}
3	N1, 1.76×10^{-4}; N2, 3.59×10^{-3}	N1, 7.46×10^{-6}; N2, $<1\times10^{-6}$; N3, 1.84×10^{-3}	N1, 4.45×10^{-4}; N2, $<1\times10^{-6}$; N3, 6.07×10^{-3}	N1, 1.57×10^{-5}; N2, $<1\times10^{-6}$; N3, 2.38×10^{-3}
4	N1, 8.63×10^{-5}; N2, 2.31×10^{-3}	N1, 2.48×10^{-3}; N2, 4.26×10^{-3}; N3, 4.37×10^{-2}; N4, 4.01×10^{-2}	N1, 2.02×10^{-3}; N2, 3.71×10^{-3}; N3, 3.75×10^{-2}; N4, 4.58×10^{-2}	N1, 1.97×10^{-5}; N2, 5.01×10^{-5}; N3, 3.23×10^{-2}; N4, 1.37×10^{-2}
5	N1 & N2, $<1\times10^{-6}$	N1 & N2, $<1\times10^{-6}$	N1 & N2, $<1\times10^{-6}$	N1 & N2, $<1\times10^{-6}$
6	N1, 9.94×10^{-4}; N2, 1.53×10^{-2}	N1, 1.50×10^{-3}; N2, 3.45×10^{-2}	N1, 1.67×10^{-3}; N2, 2.61×10^{-2}	N1, 1.04×10^{-3}; N2, 3.91×10^{-2}
7	N1, 8.79×10^{-4}; N2, 3.90×10^{-2}	N1, 6.32×10^{-3}; N2, 4.22×10^{-2}	N1, 4.80×10^{-3}; N2, 3.87×10^{-2}	N1, 6.94×10^{-3}; N2, 3.72×10^{-2}
8	N1 & N2, $<1\times10^{-6}$	N1 & N2, $<1\times10^{-6}$	N1 & N2, $<1\times10^{-6}$	N1 & N2, $<1\times10^{-6}$
9	N1, 1.38×10^{-2};	N1, 1.04×10^{-2};	N1, 6.52×10^{-3};	N1, 9.04×10^{-3};

	N2, $3.67×10^{-2}$	N2, $3.49×10^{-2}$	N2, $2.98×10^{-2}$; N3, $<1×10^{-6}$	N2, $1.62×10^{-2}$; N3, $<1×10^{-6}$
10	N1, N/A	N1, N/A	N1, $1.96×10^{-5}$; N2, $2.97×10^{-5}$	N1, $<1×10^{-6}$; N2, $1.51×10^{-5}$
11	N1, $3.55×10^{-3}$; N2, $3.63×10^{-2}$	N1, $5.87×10^{-4}$; N2, $1.80×10^{-2}$; N3, $<1×10^{-6}$	N1, $3.29×10^{-3}$; N2, $4.28×10^{-2}$; N3, $3.94×10^{-4}$; N4, $2.43×10^{-3}$	N1, $5.36×10^{-4}$; N2, $2.79×10^{-2}$; N3, $1.96×10^{-6}$; N4, $2.25×10^{-2}$
12	N1, $2.42×10^{-3}$; N2, $2.47×10^{-2}$; N3, $4.74×10^{-4}$	N1, $3.02×10^{-3}$; N2, $1.25×10^{-2}$; N3, $1.54×10^{-3}$; N4, $1.54×10^{-2}$	N1, $4.68×10^{-5}$; N2, $9.84×10^{-3}$; N3, $2.41×10^{-4}$; N4, $1.94×10^{-3}$; N5, $3.64×10^{-2}$	N1, $4.19×10^{-3}$; N2, $3.36×10^{-2}$; N3, $5.76×10^{-5}$; N4, $1.32×10^{-2}$; N5, $4.27×10^{-3}$
13	N1, $1.45×10^{-3}$; N2, $<1×10^{-6}$	N1, $2.64×10^{-4}$; N2, $3.62×10^{-2}$; N3, $6.81×10^{-3}$	N1, $4.85×10^{-3}$; N2, $2.38×10^{-2}$; N3, $2.66×10^{-3}$; N4, $3.44×10^{-2}$	N1, $4.88×10^{-3}$; N2, $3.29×10^{-2}$; N3, $3.35×10^{-3}$; N4, $4.14×10^{-2}$
14	N1, $1.59×10^{-4}$; N2, $1.21×10^{-2}$	N1, $2.53×10^{-3}$; N2, $2.77×10^{-2}$; N3, $3.17×10^{-4}$	N1, $4.01×10^{-3}$; N2, $4.18×10^{-2}$; N3, $1.15×10^{-5}$	N1, $1.52×10^{-3}$; N2, $4.32×10^{-2}$; N3, $2.87×10^{-6}$
15	N1, N/A	N1, N/A	N1, N/A	N1, N/A
16	N1, $<1×10^{-6}$; N2, $2.57×10^{-5}$; N3, $2.45×10^{-3}$	N1, $1.58×10^{-3}$; N2, $5.50×10^{-3}$; N3, $4.54×10^{-2}$; N4, $4.07×10^{-2}$	N1, $3.21×10^{-3}$; N2, $1.54×10^{-3}$; N3, $3.46×10^{-2}$; N4, $3.36×10^{-2}$	N1, $6.39×10^{-4}$; N2, $7.58×10^{-3}$; N3, $3.83×10^{-2}$; N4, $3.76×10^{-2}$

Supplementary Video 1 | Full 3D NeuE/neuron interface. 360º-rotation video of the full 3D NeuE/neuron interface shown in Fig. 1d. Green and red colors represent neurons and NeuE, respectively.

Supplementary Video 2 | Structurally indistinguishable NeuE/neuron interface. Video showing depth-coding structures corresponding to Fig. 1f, II, highlighting structural indistinguishability between neuron neurites and NeuE neurite-like interconnects.

Supplementary Video 3 | Junction between neuron neurites and NeuE neurite-like interconnects. Video showing channel-coding and depth-coding structures corresponding to Fig. 1f, III and IV, highlighting closely contacted junction between neuron neurites and NeuE neurite-like interconnect.

References

53   Steif, P. S. *Mechanics of Materials*. (Pearson, Upper Saddle River, NJ, 2012).

54   Giang, T. P. *et al.* Mechanical and electrical properties of polycarbonate nanotube buckypaper composite sheets. *Nanotechnology* **19**, 325705 (2008).

55   Hong, G. *et al.* A method for single-neuron chronic recording from the retina in awake mice. *Science* **360**, 1447-1451 (2018).

56   Henze, D. A. *et al.* Intracellular Features Predicted by Extracellular Recordings in the Hippocampus In Vivo. *J. Neurophysiol.* **84**, 390-400 (2000).

57   Du, J. *et al.* High-Resolution Three-Dimensional Extracellular Recording of Neuronal Activity With Microfabricated Electrode Arrays. *J. Neurophysiol.* **101**, 1671-1678 (2009).

58   Peden, C. S. *et al.* Striatal Readministration of rAAV Vectors Reveals an Immune Response Against AAV2 Capsids That Can Be Circumvented. *Mol. Ther.* **17**, 524-537 (2009).